Technische Universität Braunschweig

emg

Jinni Lee

Programmable Josephson Arrays for Impedance Measurements

Dissertation
Braunschweig 2010

Berichte aus dem **Institut für Elektrische Messtechnik und Grundlagen der Elektrotechnik**

Band 34

Hrsg. Prof. Dr. Meinhard Schilling

Programmable Josephson Arrays for Impedance Measurements

Von der Fakultät für Elektrotechnik, Informationstechnik, Physik der
Technischen Universität Carolo-Wilhelmina zu Braunschweig

zur Erlangung der Würde
eines Doktor-Ingenieurs (Dr.-Ing.)

genehmigte Dissertation

von
Jinni Lee

aus (Geburtsort):	Singapur
eingereicht am:	29.04.2010
mündliche Prüfung am:	24.08.2010
Referenten:	Prof. Dr. rer. nat. Meinhard Schilling
	PD Dr. rer. nat. Uwe Siegner

2010

Abstract

An innovative way of networking two programmable Josephson arrays generating synchronous waveforms for impedance ratio measurements, as the first of its kind, is presented. This pioneering approach of the Josephson Impedance Bridges is far more flexible than conventional bridges at the same level of measurement uncertainty. Results prove that aside from having the capability of measuring over a wider frequency range, the Josephson bridge permits measurements on two impedances with any value of phase angle between them.

In the two-terminal-pair Josephson bridge setup, measurements are made for a 1:1 resistance ratio at the 10-kΩ level in the frequency range between 25 Hz and 10 kHz. Uncertainties reach to levels of better than a few parts in 10^8 and results agree to the values measured from conventional impedance bridges.

Two methods for four-terminal impedance measurements have been investigated, the potential comparison circuit and the coaxial setup. Both methods are capable of measuring from DC to 6 kHz with uncertainties to 10^{-8}. The four-terminal-pair coaxial setup has potential to decrease the relative uncertainty down to 10^{-9} once systematic errors are analyzed and canceled.

Thermal converter measurements have been made to investigate the effects of transients on stepwise approximated sinewaves. Rms measurements show that transients limit the uncertainty to about 10^{-6} at 1 kHz. A simple model with an equivalent time constant is presented to evaluate the influence of different parameters on the shape of the transients. It has been experimentally established, at the 10^{-8} level of uncertainty for the determination of impedance ratios, that the variations of the transients in stepwise approximated waveforms can be neglected when using the fundamental component of rectangular waveforms.

Quantization at up to 10 kHz has been confirmed by varying the bias current of the Josephson arrays resulting in constant resistance ratios within the measurement resolution.

Kurzfassung

Ein innovativer Weg, zwei programmierbare Josephson-Schaltungen für Impedanz-Verhältnismessungen zu verknüpfen, wird erstmals in dieser Arbeit präsentiert. Dieser neuartige Ansatz einer Josephson-Impedanzmessbrücke ist flexibler als konventionelle Impedanzmessbrücken bei gleicher Messunsicherheit. Es wird gezeigt, dass neben der Möglichkeit, über einen wesentlich größeren Frequenzbereich zu messen, die Josephson-Impedanzmessbrücke auch Messungen sehr unterschiedlicher Impedanzverhältnisse und beliebiger Phasenwinkel erlaubt.

In einer Zwei-Tor-Anordnung der Josephson-Impedanzmessbrücke wurden Messungen für ein 1:1 Widerstandsverhältnis bei 10 kΩ im Frequenzbereich von 25 Hz bis 10 kHz durchgeführt. Die Ergebnisse stimmen mit denen einer konventionellen Messbrücke im Rahmen der Unsicherheit von wenigen 10^{-8} überein.

Für eine Vier-Tor-Anordnung wurden zwei unterschiedliche Methoden untersucht, eine Spannungsverhältnisschaltung und eine koaxiale Vier-Tor-Anordnung. Letztere hat das Potential, Unsicherheiten von 10^{-9} zu erreichen, sobald systematische Fehler eliminiert sind.

Um Effekte der Transienten in stufenförmig approximierten Sinuswellen zu untersuchen, wurden Messungen an Thermokonvertern durchgeführt. Diese Effektivmessungen zeigen, dass Transienten die relative Messunsicherheiten auf etwa 10^{-6} bei einer Frequenz von 1 kHz beschränken. Es wird ein einfaches Modell vorgestellt, das die Form der Transienten in Abhängigkeit der wesentlichen Parameter beschreibt. Experimentell konnte bei Impedanzverhältnismessungen mit einer relativen Messunsicherheit von 10^{-8} nachgewiesen werden, dass die Variation der Transienten in stufenförmig approximierten Wellenformen vernachlässigbar ist, wenn die fundamentale Komponente eines Rechtecksignals verwendet wird. Quantisierte Plateaus wurden bis zu Frequenzen von 10 kHz gefunden, bei denen die Variation des angelegten Stroms durch die Josephson-Schaltungen keine Veränderung des Impedanzverhältnisses zur Folge hatte.

Contents

List of Figures

Chapter 1

Introduction

In the field of metrology, the dissemination of electrical impedances has been dependent on transformer based impedance bridges for decades. The present state-of-the-art bridges allow measurements of impedances at an accuracy of 10^{-9}. A typical setup of such a bridge uses a series of sources, voltage dividers and detectors to relate impedance standards to the quantum Hall resistance [1]. However such bridges are limited to the comparison of impedance values of fixed ratios, such as 1:1 or 1:10, and at a fixed phase of 0° or 90°. These bridges operate best in the frequency range from about 0.5 kHz up to 10 kHz bounded by the limitations of inductive voltage dividers at low frequencies and at high frequencies due to increasing type-A uncertainty in null detectors.

The capability of investigating the frequency dependence in impedances became increasingly important, especially towards low frequencies, as electrical units are defined for their DC values. For example the Electron Counting Capacitance Standard (ECCS) requires the precise capacitance measurement of a cryo-capacitor in terms of the Quantum Hall resistance (R_K) at 0.01 Hz to 1 kHz with a relative uncertainty no greater than 10^{-7} [2]. Saturation effects in the ac bridges used presently, limit the uncertainty of the capacitance measurements below 50 Hz to 10^{-6}.

For more than two decades, Josephson voltage standards (JVS) have been widely used in the realization of the DC volt by national metrological laboratories throughout the world. DC voltage at 10 V level can be reproduced with an accuracy of 1 part in 10^9 or even better [3]. Based on conventional Josephson arrays these standards have also been used to measure DC resistance ratios [4].

The Josephson potentiometer based on new programmable Josephson arrays [5] has been demonstrated to measure resistance ratios near 1:1 with uncertainties of a few parts in 10^9 [6]. Considerable progress has been made since that time in the application of binary Josephson arrays towards quantum based AC voltage standards in AC electrical metrology [7–14].

By rapidly switching a series of Josephson junctions between their quantized voltage steps, AC waveforms with calculable rms voltages can be generated [11]. The accuracy is, however, largely dependent on the transients that occur during switching between quantized output voltages and their reproducibility, so far not better than $1{\cdot}10^{-6}$ at 1 kHz for rms values. Modeling and understanding the transients will be necessary to improve the precision of synthesizing Josephson stepwise approximated sinewaves [Jinni-2] [15].

Two Josephson waveform synthesizers can be arranged together with a pair of resistance standards to form a Josephson impedance bridge. Besides being a quantum based standard, a Josephson impedance bridge would offer several advantages such as operating at arbitrary frequencies, phase angles and ratios for impedance comparisons. Frequencies are adjustable in an extensive range of DC to 125 kHz in steps of mHz. Unlike present impedance measurement setups, the measurement accuracy of a Josephson bridge improves towards lower frequencies (i.e. < 1 kHz). Impedances with arbitrary phase angles can be measured by a Josephson impedance bridge through synchronization of bias electronics between two Josephson systems. For that reason, one same setup would be adequate for comparing impedances of different phases. Furthermore, programmable Josephson standards have the flexibility to switch to any voltage from steps of $\approx$150 μV up to 10 V. A Josephson impedance bridge would have the freedom to measure unconventional impedance ratios that is never experienced by traditional ac bridges.

Another advantage of a Josephson impedance bridge is its ability to be completely automated without losing accuracy due to relays and switches. Not only does this mean reduction in human operation errors, conservation of manpower and hence saving cost - it also outperforms manually operated bridges in terms of fast and accurate result collection.

Chapter 2 provides an overview of the theory of operation on Josephson arrays and impedance bridges, including models for the analysis of error contributions. Chapter 3 describes the measurement setup such as Josephson arrays and bias electronics used within this work. The measurements of transients in stepwise synthesized sine waves are presented under Chapter 4. The two-terminal and four-terminal Josephson impedance bridges and the results obtained are discussed in Chapter 5.

Chapter 2

Fundamentals

2.1 Josephson Effect

The Josephson effect is the phenomenon of tunneling electron pairs across a thin insulating barrier (on the order of a few nanometers thick) separated by two weakly coupled superconductors. This means that all Cooper pairs are in the same quantum-mechanical state and can be described by one wave function. The structure of two superconductors linked by a non-superconducting barrier material, is known as a Josephson junction; the current that crosses the barrier is the Josephson current. This effect was predicted by Brian David Josephson in 1962 [16].

With the Josephson effect an exact conversion between voltage and frequency can be produced. Since the frequency is already been defined precisely by the cesium standard [17], the Josephson effect is hence used in metrological areas for defining the volt.

2.1.1 Josephson Equations

There are two basic equations that describe the Josephson effect. 1) The superconducting phase evolution equation

$$U(t) = \frac{\hbar}{2e}\frac{\partial \phi}{\partial t} \tag{2.1}$$

and 2) the Josephson or weak-link current-phase relation

$$I(t) = I_{\mathrm{C}} sin(\phi(t)) \tag{2.2}$$

where $U(t)$ and $I(t)$ are the voltage and current across the Josephson junction, $\phi(t)$ is the difference in phase factor across the junction. I_{C} is the critical current and characterizes the largest possible dc supercurrent flowing through the junction.

The Josephson junction behaves just like a voltage driven, high frequency oscillator. The rate of magnetic flux quanta (Φ_0) being transferred perpendicular to the junction is equivalent to the drop of dc voltage over the junction.

The Josephson frequency can be modulated when an electro-magnetic field of frequency f_e (f_e in the microwave range of the spectrum) is applied to the junction using an external generator. The junction displays non-linear current voltage attributes and shows steps of constant voltages, or better known as Shapiro steps. [18]

$$V_n = n\Phi_0 f_e \tag{2.3}$$

n=1,2,3... is the number of the voltage step. The Josephson constant $K_\mathrm{J} = (\Phi_0)^{-1} = (h/2e)^{-1}$ is used instead of $(\Phi_0)^{-1}$ in metrology such that

$$V_n = \frac{nf}{K_\mathrm{J}} \tag{2.4}$$

where the value of K_J has been defined as $K_{\mathrm{J}-90} \equiv$483597.9 GHz/V since 1990.

This equation shows that the uncertainty of the microwave's frequency coupled to the Josephson junction causes the theoretical uncertainty on the voltage steps [19]. Due to modern cesium based atomic clocks, the frequency uncertainty is at a considerable range of 10^{-14} to 10^{-16}. This can be taken as the acquired uncertainty of a Josephson voltage standard. In DC metrological areas, voltage can be reproduced at a relative uncertainty of up to 10^{-11} due to thermal EMF and noise at room temperature.

2.1.2 RCSJ Model

A practical current biased Josephson junction can be described as a parallel circuit of a normal conducting resistor (junction resistance R_n), a capacitor C, and the ideal Josephson junction J. Figure 2.1 shows the schematic of the Stewart-McCumber model [20; 21]. When the circuit is irradiated by external microwave, the total current flow through the circuit can thus be characterized by

$$I_0 + I_1 \sin \omega_\mathrm{e} t = I_\mathrm{C} + I_\mathrm{R} + I_\mathrm{J} \tag{2.5}$$

The currents can be described by:

$$I_C = C\frac{\mathrm{d}V(t)}{\mathrm{d}t}, I_\mathrm{R} = \frac{V(t)}{R_\mathrm{n}}, I_\mathrm{J} = I_\mathrm{C} \sin \varphi \tag{2.6}$$

where I_0 is a dc current that is biasing the circuit.

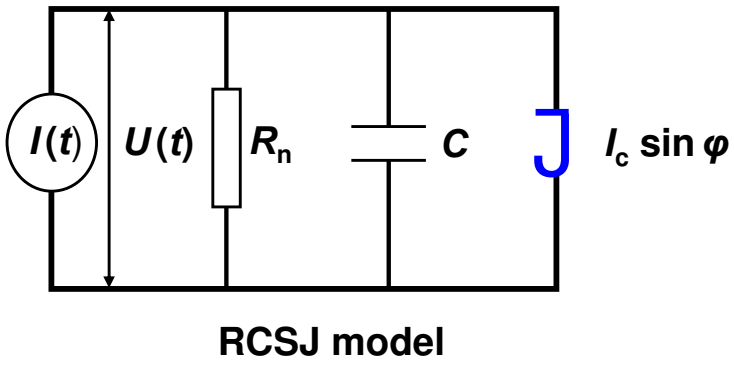

Figure 2.1: Stewart-McCumber model: a real Josephson junction can be described by a parallel circuit of a normal conducting resistor (junction resistance R_{N}), a capacitor C, and the ideal Josephson junction J.

From the Josephson equations, we can derive the following where the coefficient β_C stands for the Stewart-McCumber parameter.

$$\beta_{\mathrm{C}} = \frac{2e}{h} \cdot I_{\mathrm{C}} \cdot R_{\mathrm{n}}^2 \cdot C \tag{2.7}$$

β_{C} characterizes the quality of the Josephson resonator or similarly the attenuation of the LC circuit. The Josephson junction can be described as an inductance according to

$$L_{\mathrm{J}} = \frac{\Phi_0}{2\pi I_{\mathrm{C}}} = \frac{\hbar}{2eI_{\mathrm{C}}} \tag{2.8}$$

β_{C} can be expressed by the ratio between the characteristic frequency ω_{c} of a Josephson junction and its plasma frequency ω_{p},

$$\sqrt{\beta_{\mathrm{C}}} = \frac{\omega_{\mathrm{c}}}{\omega_{\mathrm{p}}} \tag{2.9}$$

where

$$\omega_{\mathrm{c}} = \frac{2\pi I_{\mathrm{C}} R_{\mathrm{n}}}{\Phi_0}, \omega_{\mathrm{p}} = \sqrt{\frac{2\pi I_{\mathrm{C}}}{\Phi_0 C}}. \tag{2.10}$$

and ω_c and ω_p are linked to the RC time constant $\tau_{RC} = R_n C$ as:

$$\omega_{\mathrm{RC}} = \frac{1}{\tau_{\mathrm{RC}}} = \frac{\omega_{\mathrm{p}}^2}{\omega_{\mathrm{c}}} \tag{2.11}$$

When $\beta_{\mathrm{C}} \gg 1$, a high capacitance C and a high resistance R_{n} lead to a small attenuation and subsequently to a large hysteresis of the current-voltage characteristics of the Josephson junction. A significant under-damping appears in unshunted SIS Josephson junctions commonly found in conventional voltage standard circuits. [22]

Whereas when $\beta_C \ll 1$, a zero or a negligibly small capacitance C and a low resistance R_n lead to a high attenuation and a current-voltage characteristics nearly free of hysteresis. This is a common characteristics of the over-damped SNS junctions, which will be described later as the use of programmable array for AC voltage standards.

$\beta_C \approx 1$ is found in shunted SIS junctions and SINIS junctions that are both used for voltage standard circuits. In this case, the hysteresis parameter is adjusted carefully such that the current-voltage characteristic is free from any hysteresis. [22]

2.2 Josephson Voltage Standards

A decade after the Josephson effect was predicted, it was proven around the world that the Josephson effect is confirmed for all materials and for all kinds of junctions as long as the previously stated conditions are fulfilled [23–25]. Since then the Josephson effect has found a wide range of usage in the metrological purposes. Due to the previously mentioned fact that it allows exact conversion between frequency and voltage, it is hence used in precision metrology to provide the definition of a volt.

Prior to the standardization of the Josephson junction voltage standard, national metrology institutes used specially constructed batteries, the Weston standard cell, to maintain the volt. At the beginning when the Josephson effect was introduced, small voltages generated by quantum voltage elements, at the range of millivolts, were realized by many laboratories. Notwithstanding small output voltages and complex procedures, the small uncertainty achieved in the reproduced quantum voltages surpassed immensely all other traditional voltage standards. A decade later, the fabrication of many Josephson junctions connected in series became feasible by the advance in modern semiconductor fabrication technology.

Modern 1 to 10 V DC references have progressed to be based on arrays combining 2000 - 20000 Josephson junctions in series that are irradiated by a microwave with a typical frequency of approximately 70 GHz [26–28].

DC voltage reference standards are generally based on underdamped junctions of Superconductor - Insulator - Superconductor (SIS) junctions with a McCumber parameter value $\beta_C > 1$ as described in the previous section in equation 2.7. Figure 2.2a shows the current-voltage (or IV) characteristics for an underdamped Josephson array under microwave irradiation. The highly hysteretic behavior can be seen by observing the quantized voltage across the junction that can exist without DC bias current. These voltage steps are thus called the zero-crossing steps.

One advantage of having zero-crossing steps is the absence of bias current making the output voltage insensitive to unwanted additional series resistances. Also, the fabrication process is more straightforward since the damping resistance can be ignored. However, the downside to underdamped junctions is that they are very sensitive to environmental interference. The output voltage heavily depends on the initial conditions of the dynamic equations describing the system instead of a set of bias parameters. To prevent interference causing unnecessary transitions between voltage steps, electromagnetic shielding criteria have to be followed strictly.

The drawbacks of underdamped junctions have lead to development of programmable Josephson arrays based on overdamped junctions [5]. Suitable overdamped junctions are

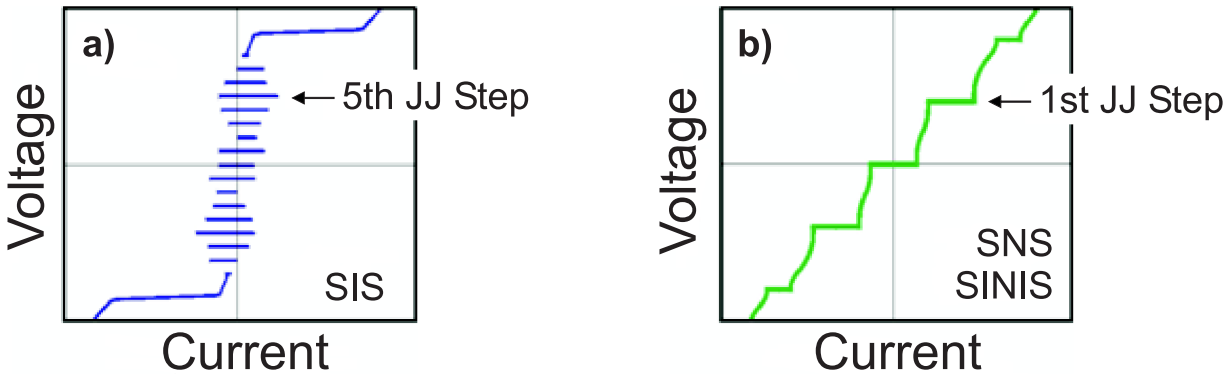

Figure 2.2: A schematic IV curve of Josephson voltage standard where (a) contains underdamped junctions from the SIS arrays and (b) overdamped junctions from arrays such as the SINIS or the SNS

found to be Superconductor-Normal-Superconductor (SNS) [29] or Superconductor-Insulator-Normal-Insulator-Superconductor (SINIS) junctions [30]. An example IV curve from such an array, shown in Figure 2.2b, demonstrates steps of constant voltage that can be biased by the driving current. It has since opened up a field of possible applications such as the use of binary programmable Josephson junction arrays for instance for many AC applications.

2.2.1 Josephson Arrays

The systems were setup using 1 V SINIS and SNS arrays of 8192 Josephson junctions. A binary divided array is used, where the number of junctions follows a binary sequence of 16 segments. With the irradation of microwaves at approximately 70 GHz, a voltage of 1.19 V can be obtained from the array. Figure 2.3 shows the layout of a conventional 1-V SINIS Josephson array, where 8192 Josephson junctions are arranged in the parallel striplines for guiding the microwaves.

The arrays were attached to the end of a cryoprobe that ran 16 coaxial cables connecting to each binary segment of the array. This end of the probe is to be placed into liquid Helium at a temperature of 4 K, while the cables will lead up to room temperature onto a connection panel at the top end of the probe. Power losses on the cryoprobes have been kept to a minimum by employing oversized circular waveguides.

The arrays operate with microwaves in the frequency range around 70 GHz. As a result, amplitudes of up to 1.2 V can be programmed in increments of the voltage generated by a

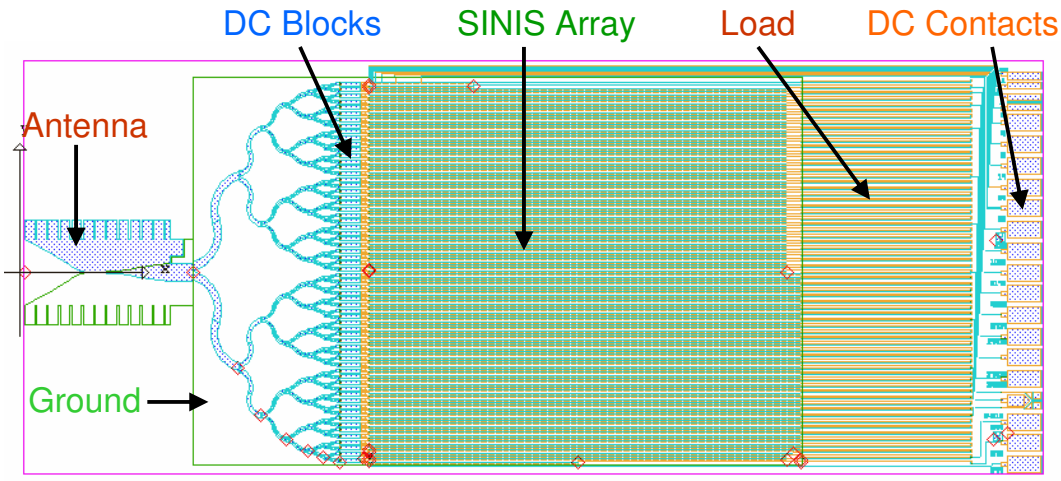

Figure 2.3: Layout of a conventional 1-V SINIS Josephson array. 8192 Josephson junctions are arranged in 14 parallel striplines. The total length of the circuit is 24mm.

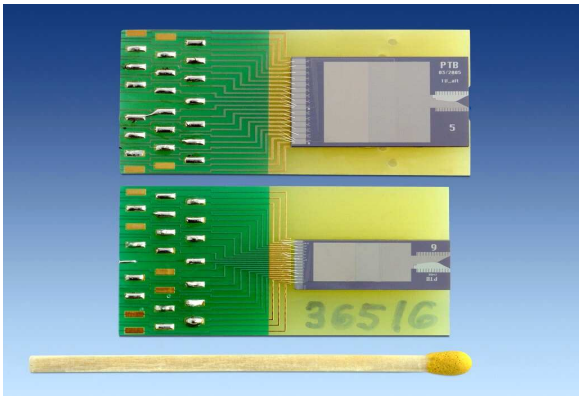

Figure 2.4: Image of two arrays of 10-V (above) with 69120 SINIS Josephson junctions and 1-V (below) with 8192 SINIS Josephson junctions

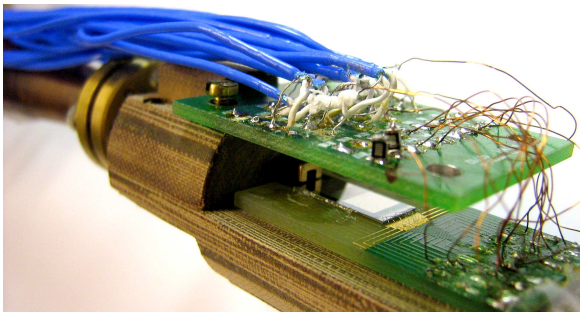

Figure 2.5: A 1-V Josephson array chip mounted and soldered on a cryoprobe end to be covered by a mu-metal shield and lowered into liquid helium at 4 K.

single junction, approximately 145 μV. In order to allow adjusting the output voltage of one of the arrays in increments smaller than these 145 μV we have used a microwave synthesizer programmable in steps of about 8 kHz which allows a resolution of 8 kHz/70 GHz $\approx$ 0.1 μV/V [31]. The maximum microwave output power is 120 mW at its center frequency of 70 GHz. Most importantly, it is directly synchronized from the 10 MHz signal of the atomic clock to attain the highest accuracy of the frequency as possible. Both frequency and power are controlled by a computer.

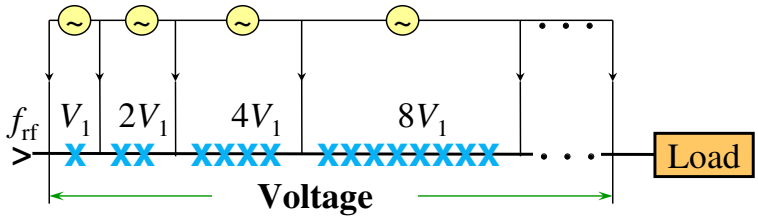

Figure 2.6: Circuit diagram of the binary segmented programmable Josephson array

2.2.2 Stepwise Approximated Waveforms

The advantage of arrays with overdamped junctions is that the voltage steps can be selected precisely and very quickly, opening up numerous applications in AC voltage generation. A new architecture has been developed for these arrays, based on a distribution of Josephson junctions in binary sequences called segments (Figure 2.6). Each of the segments irradiated at frequency f can be polarized individually on steps n = 0, 1, by applying a bias current $I_{\text{iseg}} = 0, I_{\text{stepwidth}}$(figure 2.7).

The output voltage of the array is the sum of the voltages developed by each segment, which can be calculated from the Josephson equation with the number of junctions that are activated. The possibility of controlling current sources by computer turns the Josephson junction array into a fundamental precision digital/analog converter or a programmable array [5]. By rapidly switching a series of Josephson junctions between their quantized voltage steps, AC waveforms with calculable rms voltages can be generated.

A typical programmable Josephson array is biased into 15 segments. A waveform program is performed on the bias sources to generate stepwise approximated waveforms of different samples. For example as shown in figure 2.8, a 8-sample waveform is generated with 8 steps of quantized voltage as compared to a waveform generated with 32 steps of quantized voltage. As the synthesized waveform uses higher number of samples, it appears more alike to a sine wave.

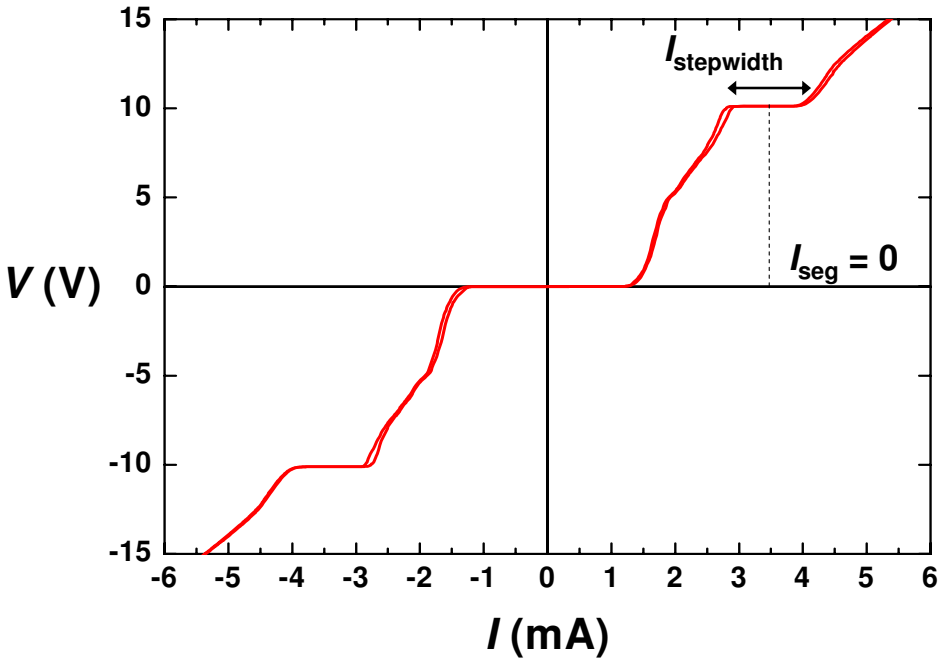

Figure 2.7: IV curve of a programmable Josephson array showing the middle of the step as $I_{\text{iseg}} = 0$

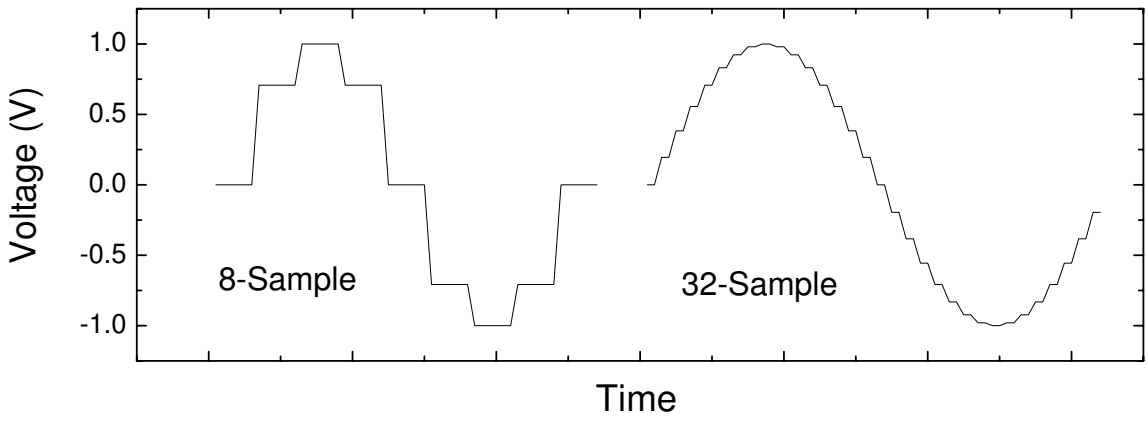

Figure 2.8: Time traces of a 8-sample and a 32-sample synthesized waveforms.

The achievable uncertainty of stepwise approximated waveforms, however, is largely dependent on the transients between quantized output voltages and their reproducibility [Jinni-2][8; 11; 15; 32].

2.2.3 Error Contributions

2.2.3.1 Transients

The primary goal of most ac applications for the Programmable Josephson Voltage System (PJVS) is to provide a signal with a precisely calculable rms value. However in practice it is not possible to completely ignore the errors caused by the transitions between quantized levels of the waveform. Figure 2.9 shows the simplified time traces of an ideal waveform and a synthesized waveform. It can be seen that the small differences caused between switching of electronics from one quantized step to the next cannot be entirely avoided. Nevertheless, it is possible to model the effect caused by the transients.

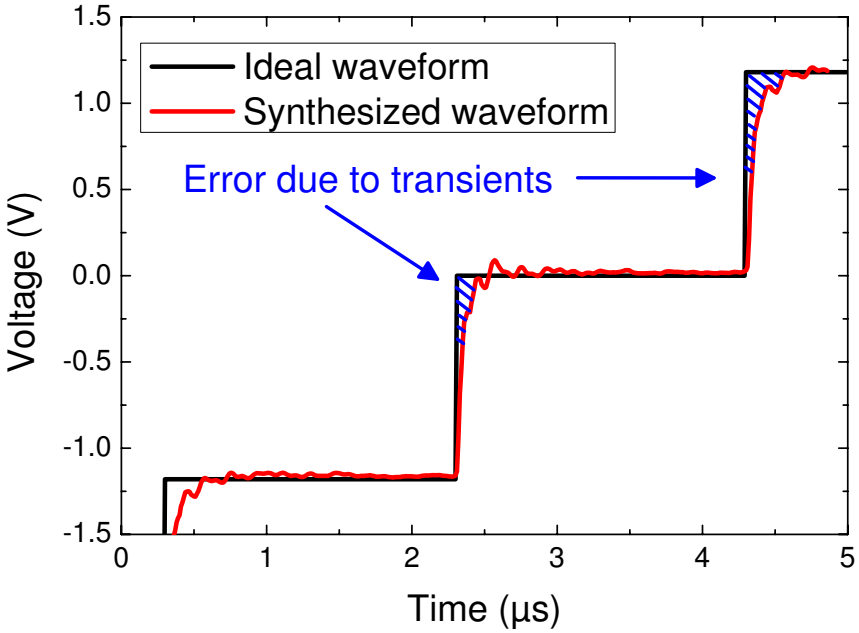

Figure 2.9: Error in a synthesized waveform due to transients that are caused by switching of electronics from one quantized step to the next.

For linear transients with $t_{\text{rise}} = t_{\text{fall}} \simeq 200$ ns, it has been calculated that the error relative to the rms voltage of the same waveform but with arbitrarily short transients, the ideal rms value, scales linearly with the number of samples per period and with synthesized

frequency [8]. This calculation was confirmed experimentally for frequencies up to 500 Hz [11].

Improvements in bias electronics gave hope that low uncertainties could be achieved also in the kHz-range due to a significant reduction in the duration of the transients [32]. At the same time, a model for the influence on the transients of the precise operating parameters of the Josephson array has been proposed [15], affecting transients through delays on the rising and falling edges of the synthesized waveform.

The initially expected reduction in the ac-dc transfer difference from the ideal value has however not been observed, motivating the development of a more detailed description of the transients and their dependence on the precise operating parameters of the Josephson array.

Pulse driven arrays seem preferable for this purpose, but unfortunately, their highest peak amplitudes achieved are still below the 1-V level [33], requiring pre-amplifiers which limit uncertainties in AC-DC transfer measurements [34].

A simple model is presented that describes the current dependence of the transients due to the equivalent capacitances in the measurement system. The measurement results qualitatively agree with this model. It is shown that the presence of asymmetries between rising and falling edges limits the dependence on the number of samples per period of the synthesized signals.

2.2.3.2 Model of Current Dependence

Figure 2.10 shows a simple model where the whole system – the output resistance of the bias source, the cables between the bias sources and the array, the output cables between the array and the measuring instrument, any filters used on any of these connections, etc—is grouped into a single RC time constant [35]. For simplicity, the bias sources, in our case voltage sources, are considered ideal step generators. It should be pointed out that this model is not deduced from the actual physical set-up.

The non-linear behavior of the array, J in figure 2.10, has been approximated by a piecewise continuous function, presented in figure 2.11. For the transients, the array can be modeled as a constant current source $I_{0\mathrm{H}}$ in parallel with the dynamic resistance of the array $r_\mathrm{d} = U_\mathrm{J}/(I_{1\mathrm{L}} - I_{0\mathrm{H}})$, where U_J is the voltage on the first order Shapiro step and $I_{n\mathrm{L}}$ and $I_{n\mathrm{H}}$ are the low and high current edges of the n-th order Shapiro step of the Josephson array. The current source accounts for the fact that any current below $I_{0\mathrm{H}}$ cannot charge the equivalent capacitance C, as the array behaves as a superconducting short circuit. In this model, the measuring instrument is connected directly across the array without any cables. For all the discussions and measurements in this paper, the positive and negative Josephson

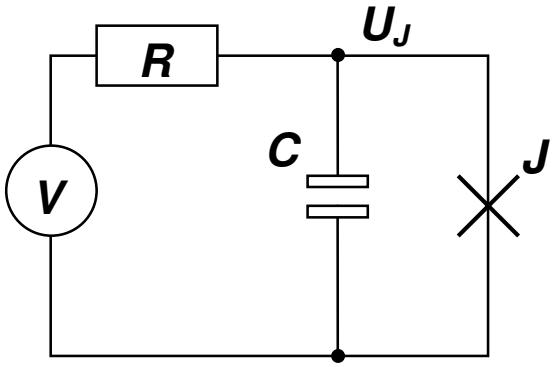

Figure 2.10: Schematic circuit diagram for the model of the system used. An ideal step voltage source switches the output voltage between the n = -1, 0, +1 steps of the Josephson junction array J. Resistance R and capacitance C model the behavior of the complete system.

steps were biased at $+I_{\mathrm{Bias}}$ and $-I_{\mathrm{Bias}}$, respectively. Note that only cases where $I_{\mathrm{Bias}} \leq I_{1\mathrm{H}}$ are considered. The zero step was biased at 0 mA.

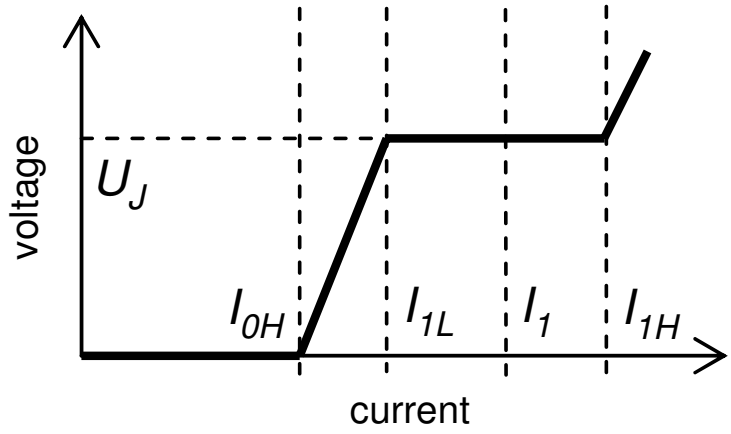

Figure 2.11: Model of the Josephson junction array with voltage step U_{J}, zero step width $2 \cdot I_{\mathrm{OH}}$ and first order step width $I_{1\mathrm{H}} - I_{1\mathrm{L}}$. I_{Bias} is the bias current at the end of the transient.

For a transient between the zero and +1 steps of the array, the ideal bias source changes output from 0 V at t=0− to U_{Bias} at t=0+. For the array to be on the first order step, $U_{\mathrm{Bias}} = U_{\mathrm{J}} + I_{\mathrm{Bias}} \cdot R$ and $I_{1\mathrm{L}} \leq I_{\mathrm{Bias}} \leq I_{1\mathrm{H}}$. This ideal voltage step is connected through R to the parallel combination of C, r_{d} and the current source I_{OH}. The first order step from the array response limits the output voltage of the Josephson Waveform Synthesizer (JWS) to U_{J}.

If r_p is the parallel combination of r_d and the equivalent source resistance R, the instantaneous output voltage of the JWS, across the capacitor and the array, for a given selected bias current on the step I_Bias can be expressed as:

$$u_\mathrm{JWS}\left(t, I_\mathrm{Bias}\right) = \min \left\{ \begin{array}{c} U_\mathrm{J} \\ \left[U_\mathrm{J} + R \cdot \left(I_\mathrm{Bias} - I_\mathrm{0H}\right)\right] \, \frac{r_\mathrm{P}}{R} \left(1 - e^{\frac{-t}{r_\mathrm{p} C}}\right). \end{array} \right. \tag{2.12}$$

The dependence on I_1Lcan be expressed explicitly, instead of through r_p, by rewriting 2.12 as:

$$u_\mathrm{JWS}(t, I_\mathrm{Bias}) = \min \left\{ \begin{array}{c} U_\mathrm{J} \\ U_\mathrm{J} \, \left[1 + \left(I_\mathrm{Bias} - I_\mathrm{1L}\right) \frac{r_\mathrm{p}}{U_\mathrm{J}}\right] \, \left(1 - e^{\frac{-t}{r_\mathrm{p} C}}\right). \end{array} \right. \tag{2.13}$$

As a result, the transient between 0 V and U_J has a duration of:

$$t_\mathrm{rise}(I_\mathrm{Bias}) = r_\mathrm{p} C \cdot \ln \frac{U_\mathrm{J} + R\left(I_\mathrm{Bias} - I_\mathrm{0H}\right)}{U_\mathrm{J}(1 - R/r_\mathrm{p}) + R\left(I_\mathrm{Bias} - I_\mathrm{0H}\right)} \tag{2.14}$$

or, to express the dependence on I_1L more clearly,

$$t_\mathrm{rise}(I_\mathrm{Bias}) = r_\mathrm{p} C \cdot \ln \left(1 + \frac{U_\mathrm{J}}{r_\mathrm{p}(I_\mathrm{Bias} - I_\mathrm{1L})}\right) . \tag{2.15}$$

Mathematically, the rise time becomes infinitely long when $I_\mathrm{Bias} = I_\mathrm{1L}$, but not for $I_\mathrm{Bias} = I_\mathrm{1L}^{+} = I_\mathrm{1L} + \varepsilon$, where ε is an arbitrarily small current. In practice, there will be an upper bound for t_rise.

The same reasoning applies to the transient between 0 V and $-U_\mathrm{J}$, which has exactly the same duration and dependence on the bias current setting $-I_\mathrm{Bias}$.

For the falling transient, the ideal bias source drops to 0 V at t=0+. As the voltage across the capacitor cannot change abruptly, the current through the array becomes I_1L immediately. After that instant, the output of the JWS follows the discharge of the capacitor through r_p until the superconducting short-circuit keeps the voltage constant. The I_OH current source is still in parallel with r_d and influences the theoretical final voltage across the capacitor. The transient from $-U_\mathrm{J}$ to the zero step thus follows:

$$u_\mathrm{JWS}(t, I_\mathrm{Bias}) = \max \left\{ \begin{array}{c} 0 \text{ V} \\ \left(U_\mathrm{J} + I_\mathrm{0H} \cdot r_\mathrm{p}\right) e^{\frac{-t}{r_\mathrm{p} C}} - I_\mathrm{0H} \cdot r_\mathrm{p} \end{array} \right. \tag{2.16}$$

and has a duration of

$$t_\mathrm{fall} = r_\mathrm{p} C \cdot \ln \left(1 + \frac{U_\mathrm{J}}{r_\mathrm{p} \cdot I_\mathrm{0H}}\right) . \tag{2.17}$$

As previously, the same reasoning applies to the transients between $-U_J$ and 0 V, which have exactly the same duration. From equations 2.16 and 2.17, it is clear that neither the transients to the zero step nor the fall time depend on the value of bias current on the step I_{Bias}.

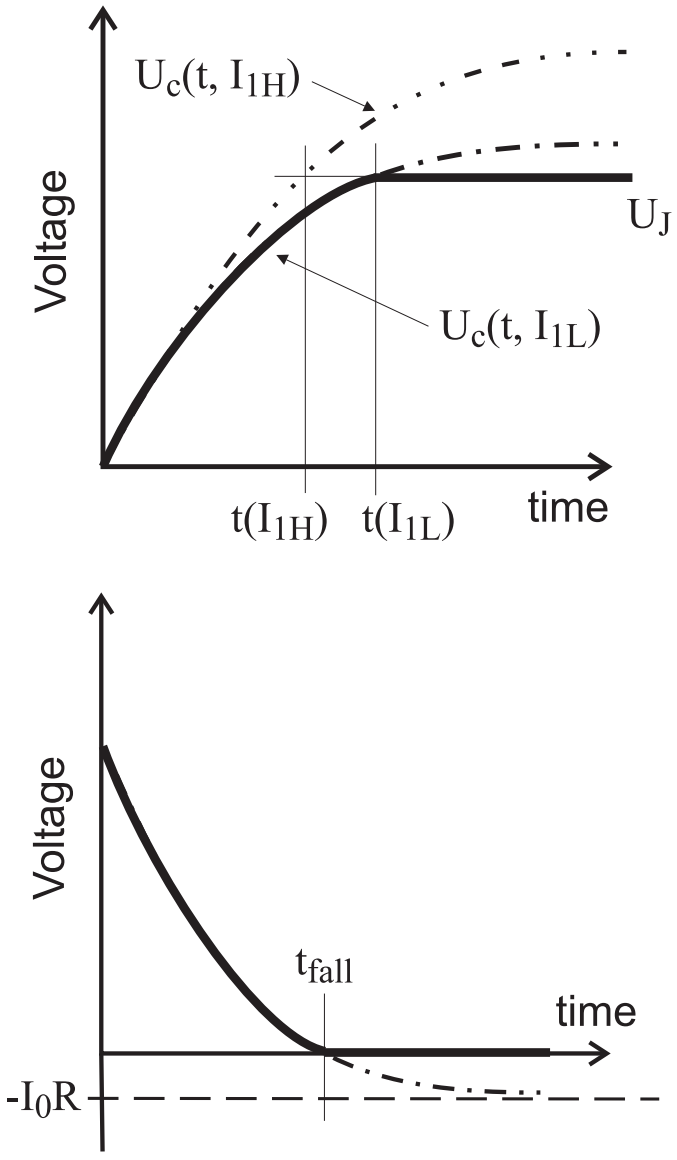

Figure 2.12: Rising (top) and falling (bottom) transients at the output of the array. The two extreme cases for the rising transients are presented, corresponding to bias currents on the edges of the first order step, I_{1H}, I_{1L}. The exponential functions without the non-linear behavior of the array are also shown, although the rising transient for I_{1L} cannot be distinguished from the Josephson voltage.

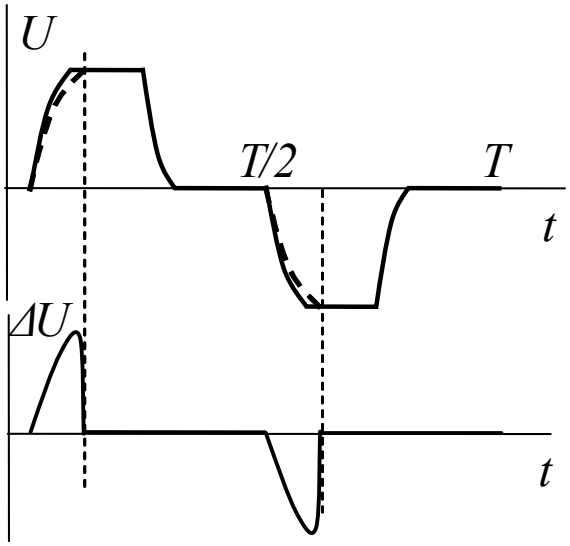

Figure 2.13: Synthesized waveforms using four samples per period and two Josephson step bias currents I, and the difference between them $\Delta U(I_1, I_2, t) = U(I_1, t) - U(I_2, t)$

The predicted transients are shown in figure 2.12. The top graph depicts the extreme cases, when the selected bias currents are at the edges of the first order step. In order to maximize the effect of the transients, the duration of the transients should be long compared to the period of the signal investigated. An approximated sine wave with four samples per period is used to study the influence of I_{Bias} and I_{OH} at high frequencies. Figure 2.13 shows the predictions according to our model for two different bias currents. The difference between the two signals is shown in the lower half and only becomes non-zero during the transients that depart from the zero Josephson step.

2.3 Conventional Impedance Standards

The impedance is commonly maintained in national measurement laboratories at the highest accuracy levels using AC Bridges, such as the equal power four-terminal pair capacitance bridge or the quadrature bridge. The Coaxial AC Bridge System uses a series of sources and detectors to relate the value of a 1 kΩ resistance standard to the 10 pF primary capacitance standard in terms of the quantum Hall resistance. More generally, a number of different bridge systems are used to enable measurement of capacitance standards in the range 1 pF to 1 mF (decade values) between 100 Hz and 10 MHz. [1]

The basis of an AC bridge is its use of coaxial conductors which carry equal and opposite currents between the inner and the outer conductors. When the currents are balanced such that they are equal and opposite, the bridge can be ensured that there is negligible external magnetic interference on the bridge system. The main sources of uncertainty in the quadrature bridge are the bridge frequency and the imbalance contributions from the harmonics in the bridge source since the bridge is frequency dependent.

A terminal point of the measuring standard can described physically as an inner and outer coaxial port, or a terminal-pair. Resistance standards that are measured in DC are made with two-terminal or four-terminal. Whereas an impedance standard, which describe a measure of opposition to alternating current, is quantified in two-terminal-pairs or four-terminal-pairs. Therefore, the bridges that are used for measurement of impedance standards are categorized into two classifications: two-terminal-pair bridges and four-terminal-pair bridges.

2.3.1 Coaxial Two-Terminal-Pair Ratio Bridge

A coaxial two terminal-pair ratio bridge is often used for comparing the ratio of two admittances with similar values. Figure 2.14 shows the basic principle of a coaxial two terminal-pair ratio bridge.

To obtain the precise ratio of two impedance standards at a nominal 1:1 ratio, voltages with a fixed ratio of approximately 1:-1 are generated by a ratio transformer and applied to the two standards. To compensate for the deviation U of the transformer ratio from nominal and for the deviation of the impedance standards from their nominal value, a voltage injection system is used to apply a small adjustable voltage U_{inj} in series with one arm of the ratio transformer.

The injected voltage is generated by an inductive voltage divider (not shown in figure 2.14) and has a typical relative uncertainty of not more than $1 \cdot 10^{-5}$. The injected voltage is adjusted until the voltage detector (usually a lock-in amplifier) is nulled.

To eliminate the deviation of the transformer ratio from nominal, the two impedance standards are interchanged and the bridge is re-balanced. Then, the voltages injected for both configurations allow calculation of the precise ratio of the impedance standards. Such a coaxial ratio bridge is best in the frequency range from about 0.5 kHz up to 10 kHz and yields a relative uncertainty of approximately $5 \cdot 10^{-9}$.

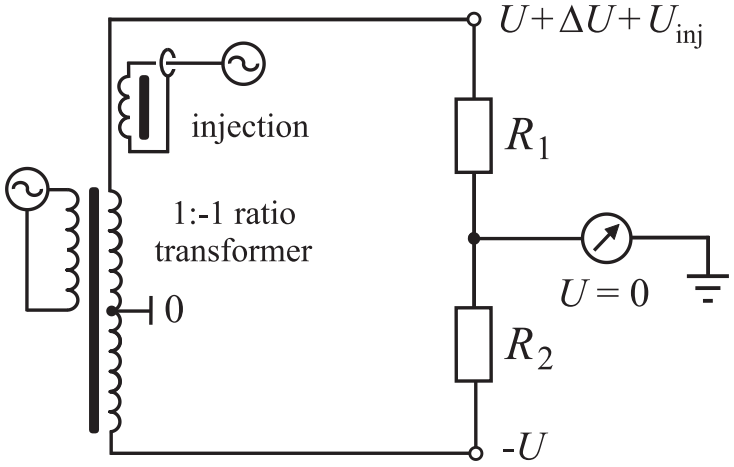

Figure 2.14: Principle of a coaxial ratio bridge for the measurement of the ratio of two impedances, R_1 and R_2. For the sake of simplicity, the outer conductors carrying the equalized return currents are not shown.

2.3.2 Four-Terminal-Pair bridges

The four-terminal-pair quadrature bridge accurately relates the value of two 100 kΩ resistance standards with two 1 nF capacitance standards at a frequency of 1.592 kHz. Since the quadrature bridge is highly frequency sensitive, the frequency of the source must be stable (or known) to an uncertainty of 10^{-9} and any contributions from the harmonics of the fundamental frequency component filtered to avoid inter-modulation distortion. Such quadrature bridges are used generally to measure the ratio between a resistance standard and a capacitance standard.

For comparisons between ratios, the four-terminal-pair ratio bridges are used. Some examples of four terminal-pair ratio bridges are the 100:1 equal power resistance bridge and the 10:1 capacitance bridge. The 100:1 equal power bridge enables accurate comparison of a 1 kΩ resistance standard with a 100 kΩ resistance standard at a frequency of 1.592 kHz. The bridge system is designed to ensure that both resistance standards only dissipate 1 mW of power during measurements.

Whereas the four terminal-pair 10:1 capacitance bridge enables accurate scaling of the value of capacitance standards at a frequency of 1.592 kHz. The combined quadrature and 10:1 capacitance bridge measurements enable the value of the 1 nF capacitance standards to be determined. This value can then be scaled up to 1mF or down to 1 pF using the 10:1 bridge system.

Chapter 3

System Components

3.1 Bias Electronics and Synchronization

A pair of current bias sources, fabricated at the National Physical Laboratory (NPL), was used for driving the dual Programmable Josephson Voltage Systems (PJVS). The specialty of such sources are their ability to create fast rise-times of less than few ns per step change. This is a huge advantage as errors of synthesized waveforms come mainly from its inability to create a perfect step with negligible rise-time.

Each bias source has 15 drive circuits for synthesizing AC waveforms, where each bit can be set to 0, +1 or -1. It has an update rate of 1.7 μs allowing up to about 1000 samples for a frequency of 1 kHz as described in [36]. The bias current can be set to any value in the range of -30 mA to + 30 mA using a fast D/A converter with 12-bit resolution. The uncertainty in the current resolution is about 0.015 mA which is sufficient for biasing an array step with a width of approximately 1 mA at a bias current of 4 mA. The bias electronics is capable of generating a trigger signal either with every change of the output channels or once per period of the synthesized waveform. A full specification is provided in appendix A.1.

To obtain the best rise-time, the bias source is designed to be used with 50-Ω loads connected between the output of each current source and the overall system shield potential, defined by the outer conductors of the coaxial cable. The control software makes a correct allowance for the current flowing in these loads, which is dependent on the array segment biases. Hence coaxial cables of 50-Ω drive impedance are chosen for connecting the source to the array as it allows termination matching to reduce crosstalk between bias channels. Rise-times between voltage steps of as low as 10 ns can be realized with the transmission line method [37], where the reflections are cancelled at the array by a short circuit at the end of a transmission line in a 50-Ω system.

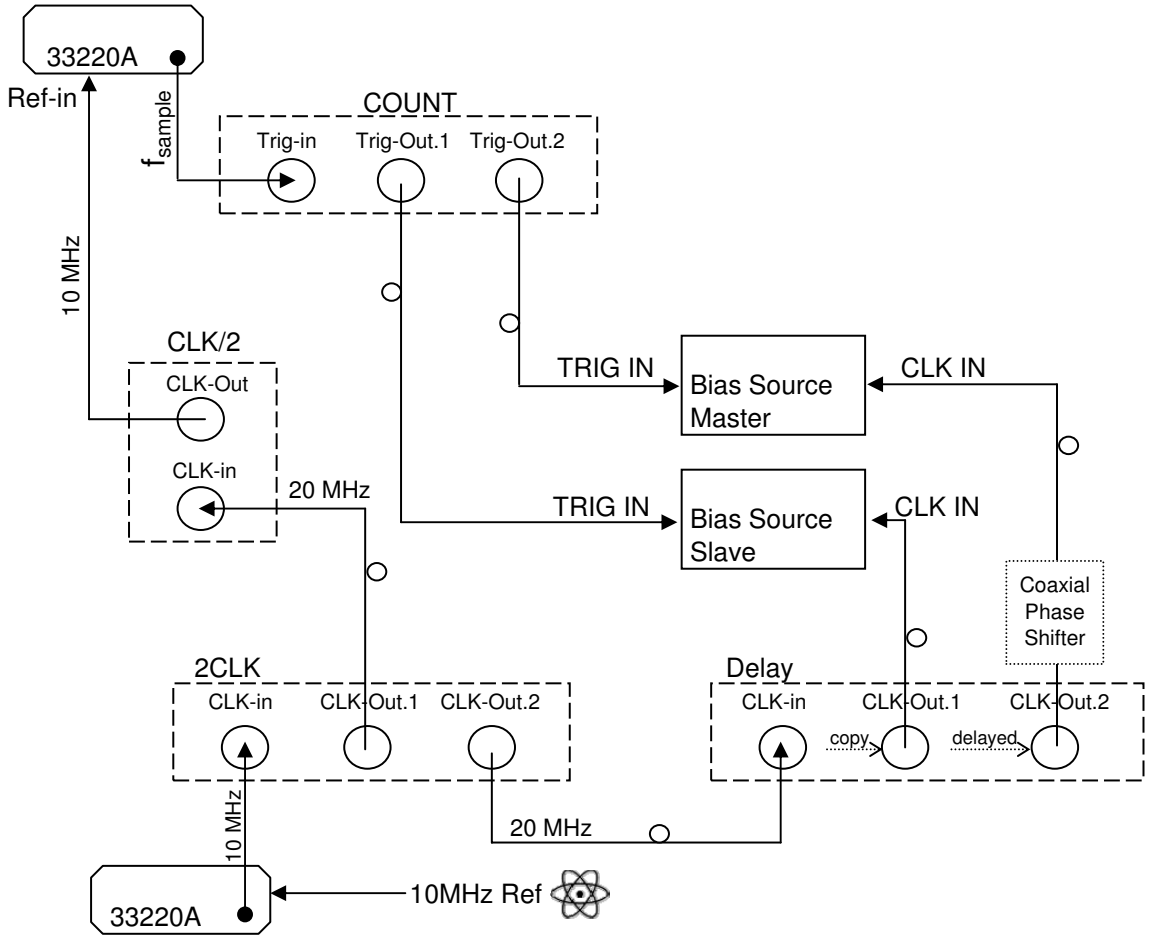

Figure 3.1: Trigger and clock scheme used for synchronizing two bias sources

A software package written in LabVIEW was specially created for running the Josephson Bridge System. In order to carry out extended flexibility in the software, the structure was oriented in a 7 layer model of computer networks. The lowest layer just transmits a byte to the bias source. One level higher uses the information that these bytes correspond to setup, voltage or time information. This concept is continued until the top most layer, which lets the user control the system. (Appendix A.2) With the software skeleton in place, it becomes easy to introduce add ons or tweaks into the system. One such example is the phase shifting between the two systems.

Since impedance measurements include quadrature measurements, it requires the Josephson Bridge System to phase shift between the two waveform synthesizer sources. Pulses from an Agilent 33220A synthesizer are used to externally trigger the two Josephson bias electronics. The output signal of one module of the bias electronics is coupled via an optical

isolation to the null detector as reference signal. The common clock that runs at 20-MHz enables a syncronous time base for all instruments.

The delay is computer controlled via an USB interface. Its resolution is 250 ps for a 50-ns range. For high frequencies, especially in the range from 1 kHz to 10 kHz, the resolution of 250 ps is insufficient. Hence an additional coaxial phase shifter having 100 ps span is used to manually set the phase between both systems to an accuracy of about 10 ps. Figure 3.1 shows the trigger and clock scheme used for synchronizing the two bias sources.

3.2 Reference Precision Resistors

A pair of 10 kΩ Vishay VHP202 resistors were chosen and constructed in to a thermal box for temperature stability to 1 mK. This type of plane network plated resistors were selected because of their high accuracies of 0.001 % and a long term shelf life of less than 2 ppm/yr. These resistors also have remarkably low residual inductance and capacitance, as would be expected from their small physical size and low-inductance construction ($< 0.08\mu$H).

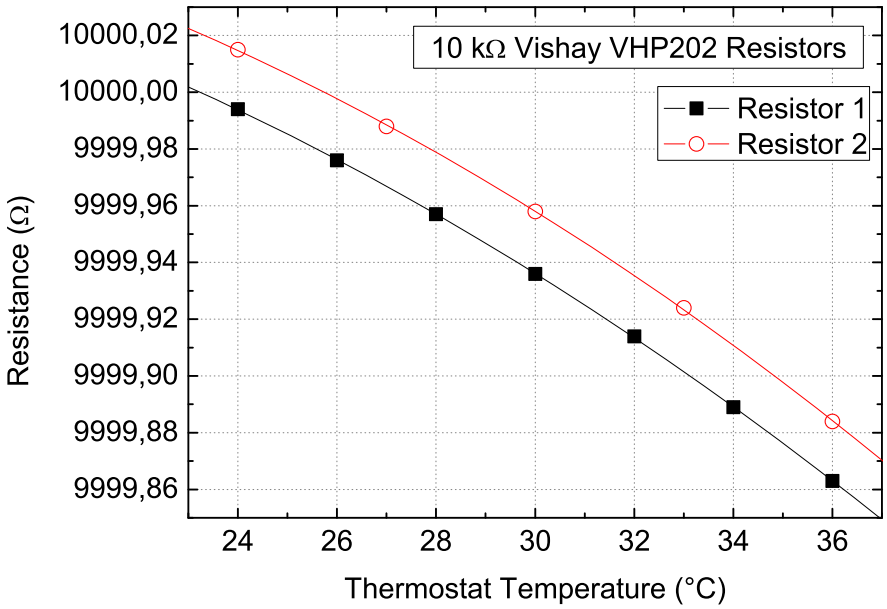

Figure 3.2: Temperature coefficient of the two Vishay resistor standards used in all setups

The two resistors used have been selected to have almost identical temperature coefficients in the temperature range 24 °C to 36 °C. Figure 3.2 demonstrated the temperature coefficient of the Vishay resistors to as low as 1 ppm/K. Furthermore, they are placed in a thermally controlled box which is maintained to 29.95 °C within 0.001 °C. Before a measurement can be made, these resistors need at least a day for their temperature to stabilize if the thermal box requires power to begin with.

The resistors were mounted in two separated chambers of one aluminum box to ensure good temperature correlation and low electrical cross coupling. (Figure 3.3) Each end of the resistor pin is divided into two lines of shielded cables out to a pair of BPO connectors. This

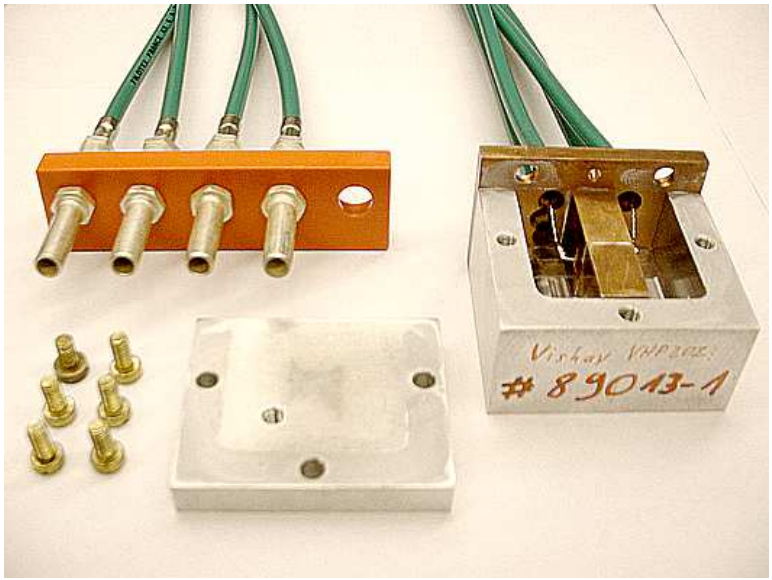

Figure 3.3: Metal enclosure for housing the actual resistors separating the resistors pins by a copper wall.

is crucial as they are the internal defining points for a four-terminal definition of the resistor standards.

The aluminum cased resistors were subsequently placed into a foamed filled metal casing that is fitted with a dozen temperature sensors. The Eurotherm 3508 hybrid programmer is used to regulate the voltage on the temperature controller to keep the inner temperature to ± 1 mK. Finally the metal casing is housed in a wooden frame with another layer of foam insulation to shield from further temperature fluctuations.

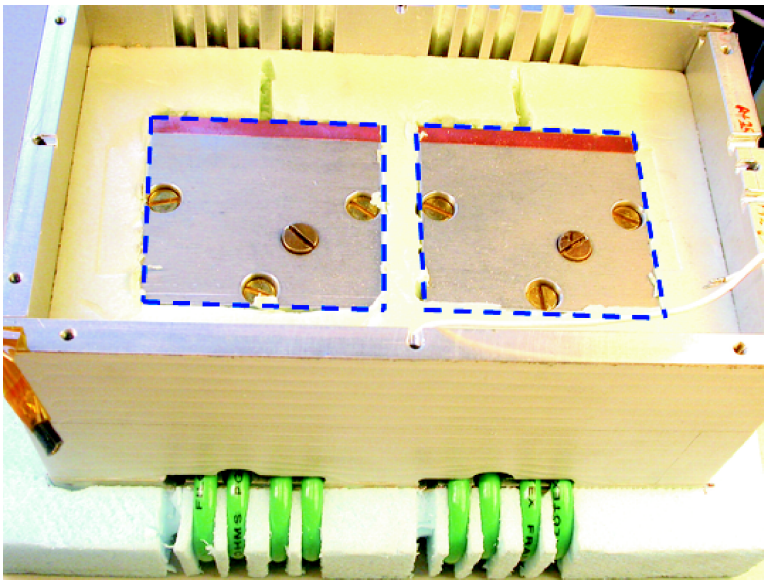

Figure 3.4: Photo of the temperature controlled box for housing the two resistors that are highlighted in blue squares.

Chapter 4

Stepwise Synthesized Josephson Sine Waves

By rapidly switching a series of Josephson junctions between their quantized voltage steps, AC waveforms with calculable rms voltages can be generated. As described previously, the main part of error contribution in the stepwise synthesized sine waves depends largely on the transients between quantized output voltages and their reproducibility [Jinni-2][8; 11; 15; 32].

This chapter presents the measurement results in comparison with the transients modelling introduced in the previous chapters.

4.1 Transient Measurements

The waveforms at the output of the JWS were acquired with a 500 MHz digital oscilloscope. Figure 4.1 shows a transient between the zero and first Josephson steps for the whole array operated as a single segment. A steep transient of 5 ns is followed by overshoot and ringing. The output settles to the quantized voltage after about 50 ns. As for most of the other measurements presented in this paper, the array had $I_{0\mathrm{H}} = 0.4\ mA, I_{1\mathrm{L}} = 2.15\ mA$ and $I_{1\mathrm{H}} = 2.75\ mA$. The dynamic resistance of the whole array for the model thus becomes r_d = 676 Ω. The bias current used was 2.3 mA. Note that the transient starts slightly after t = 0 ns, due to the setting of the oscilloscope trigger.

The grey curve in figure 4.1 shows the transient predicted by the model for R = 50 Ω and C = 120 pF. Using the minimum bias current increment from the NPL bias source, ε= 6.3 μA, the model predicts $t_{\mathrm{rise}}(I_{1\mathrm{H}})$ = 36.7 ns, $t_{\mathrm{rise}}(I^{+}_{1\mathrm{L}})$ = 80.8 ns, and t_{fall} = 39.9 ns.

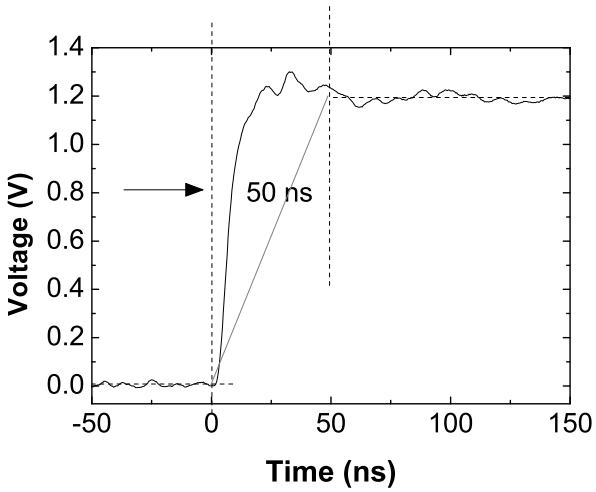

Figure 4.1: Time trace of a transient from a 100 kHz 4-sample synthesized waveform. The grey curve shows the response of the model for $R = 50\ \Omega$ and $C = 120$ pF.

4.1.1 Bias Current I_{Bias} Dependance

A detail in the waveform used for investigating the influence of the bias current setting is presented on the top half of figure 4.2. This waveform corresponds to $I_{\text{Bias}} = 2.3$ mA. The result of subtracting this waveform from $u_{\text{JWS}}(t, 2.6\ mA)$ is presented in the lower half of figure 4.2. In order to retain sufficient time resolution, only half a period is shown. As predicted by the model, (figure 2.13), the difference only becomes non-zero during the transients leaving the zero Josephson step. The peak in the difference waveform extends for about 40 ns, in agreement with the 50 ns required to reach quantization deduced from figure 4.1.

4.1.2 Josephson Step Width Dependance

From 2.14, 2.15 and 2.17, the rise and fall times depend on the width of the Josephson steps through I_{0H} and I_{1L}. These can be varied by modifying the microwave power employed. With the array used for this paper, a change from 15 mW to 45 mW (maximum power available for these measurements), results in the width of the zero step decreasing 1.5 mA to 0.3 mA and I_{OH} changing accordingly. At the same time, the first order step width increases from 0.36 mA to 0.72 mA, decreasing the value of I_{1L}. The first order steps remain centered at roughly the same current throughout.

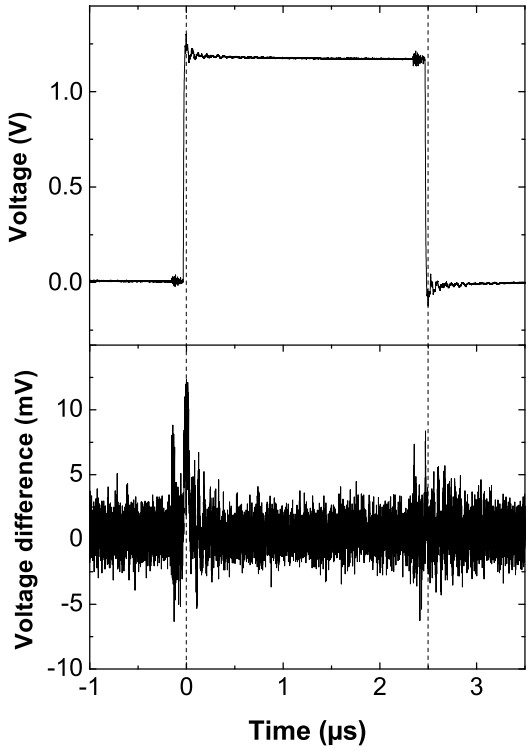

Figure 4.2: Output voltage for one bias current setting $u_{\mathrm{JWS}}(I_{\mathrm{Bias}} = 2.3mA)$ and voltage difference between two different values $\Delta u = u_{\mathrm{JWS}}(2.6mA) - u_{\mathrm{JWS}}(2.3mA)$.

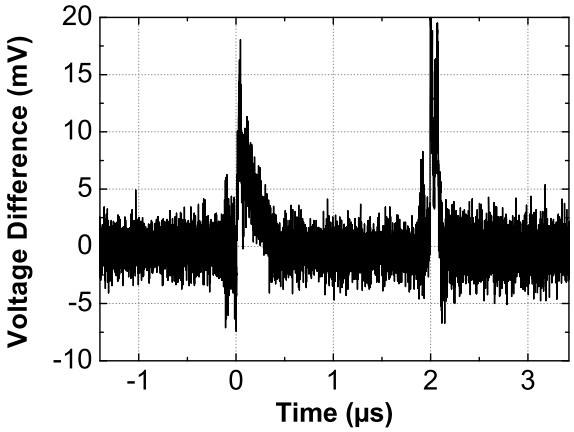

Figure 4.3: Example of the difference between the JWS output at two different widths of the Josephson steps, achieved by applying different microwave powers.

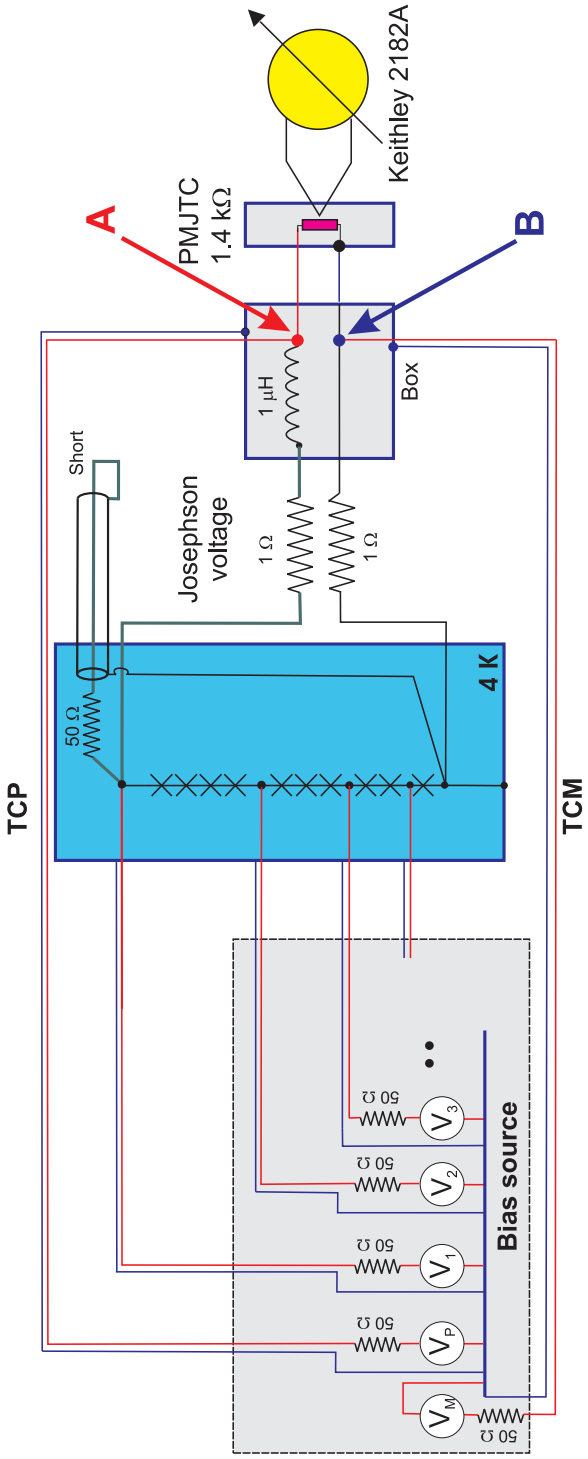

Figure 4.4: Schematic diagram of the 4-terminal Josephson waveform synthesizer, with TCP and TCM supplying the load current required by the PMJTC at the voltage set by the Josephson array. Points A and B require careful balancing to avoid inducing a current on the voltage leads.

As a result, t_{rise} becomes shorter whereas t_{fall} becomes longer as microwave power is increased. The difference between two waveforms using the same bias current setting for the first order step, but synthesized using higher and lower microwave powers will have positive peaks both at the rising and at the falling transients. Figure 4.3 shows experimental confirmation of this behavior qualitatively. It is however unclear, why the duration of the peaks in the difference waveform are now much longer. This extended differences are present in all the differences that were measured with different microwave power levels.

4.2 Thermal Converter Measurements

In order to determine the variations in rms value, the rms value of the JWS waveforms was measured using a Planar Multi Junction Thermal Converter (PMJTC). The PMJTC used has a resistance of 1.4 kΩ. In order to have the shortest transients possible, the transmission line method [37] was also used in these measurements, as shown in figure 4.4. When using a 1.2 V JWS, the current load on the bias modules exceeds their maximum output current capability at this voltage. Two additional modules in the NPL bias source are used to feed the current required by the PMJTC in a four terminal JWS [11]. The sources TCP and TCM provide an in-phase or anti-phase copy of $u_{JWS}(t, I_{Bias})$, so that ideally no current flows in the voltage leads from the Josephson array.

Non-idealities in TCP and TCM mean that careful balancing between the Josephson voltages and the PMJTC driving currents from TCP and TCM, is essential at the input of the PMJTC (points A and B in figure 4.4). In this set-up, the open circuit smallest increment in TCP or TCM of 320 μV translates into approximately 6 μV at the PMJTC. The control software in the JWS compensates for the offset and linearity error of each channel in the bias source, including TCP and TCM. The first step in the measurement procedure is to determine and compensate the offset voltage and gain of TCP and TCM. No significant drift has been observed in these two parameters for the duration of the measurements that have been taken.

There will still be an unwanted voltage difference between the PMJTC and the array. For a dc voltage, the voltage across the PMJTC is slightly different from the voltage across the Josephson array, $U_{\text{PMJTC+}} = U_{\text{JWS+}} + \delta I_+ \cdot 2\Omega$, where δI_+ is the mismatch between the difference of TCP and TCM at these output voltage settings and the Josephson array. To first order, this is also the difference in the rms value. For the opposite polarity, $U_{\text{PMJTC}-} = U_{\text{JWS}-} + \delta I_- \cdot 2\Omega$. The unwanted contribution to the difference is thus $\Delta U_{\text{PMJTC}} = \frac{1}{2}(\delta I_+ - \delta I_-) \cdot 2\Omega$, or approximately half the mismatch for each polarity. For each sample k in a stepwise approximated waveform, the rms value of the whole waveform is proportional to

$U^2_{PMJTCk} = (U_{\mathrm{JWSk}} + \delta I_k \cdot 2\Omega)^2 \approx U^2_{\mathrm{JWSk}} + U_{\mathrm{JWSk}} \cdot \delta I_k \cdot 2\Omega$. Waveforms have been investigated where the number of samples $N_{\mathrm{Samples}} = 2 \cdot \ n, n = 1, 2, ...$ and the theoretical voltages for the samples are symmetrical around 0 V. Over a period, the unwanted contributions to the rms value average out to a certain degree. It should also be noted that the measured AC-DC differences (figure 4.5)(figure 4.6) are significantly below the worst case value of 10 $\mu V/V = 2 \cdot 6\ \mu V/1.2\ V$ for extremely mismatched TCP and TCM outputs.

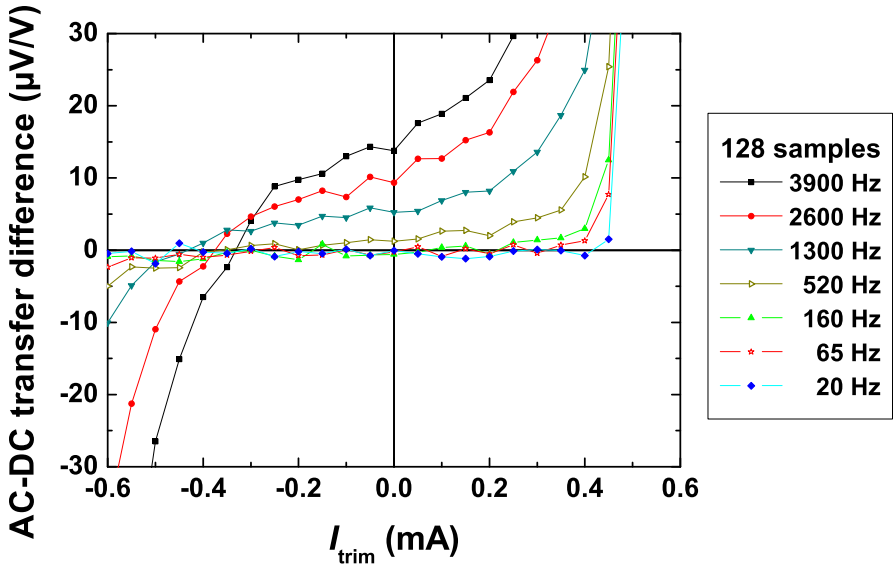

Figure 4.5: AC-DC transfer difference as a function of trim current for frequencies from 20 Hz to 3.9 kHz using 128 samples.

The PMJTC measures the difference between the stepwise approximated waveform and the rms value calculated for the same waveform but with arbitrarily short transients, the ideal rms value. A precision digital nano-voltmeter was used to measure the output of the PMJTC. As usual for AC-DC transfer measurements, a dc+ / ac / dc- sequence was followed. As a precaution, long waiting times of 90 / 60 / 60 s, respectively, were observed to allow the rms value to settle after changes in the bias parameters. In order to minimize reflections, special care was taken to ensure equal lengths for the cables connected on the output of the JWS, including the current carrying cables for TCP and TCM.

Figure 4.5 shows the transfer differences for AC-DC measurements in the frequency range from 20 Hz to 4 kHz, using 128 samples per period of the generated waveform, when the bias current is varied or trimmed from the center of the first order Josephson step. At low frequencies, the difference is constant over a wide range of bias trim currents. Increasing

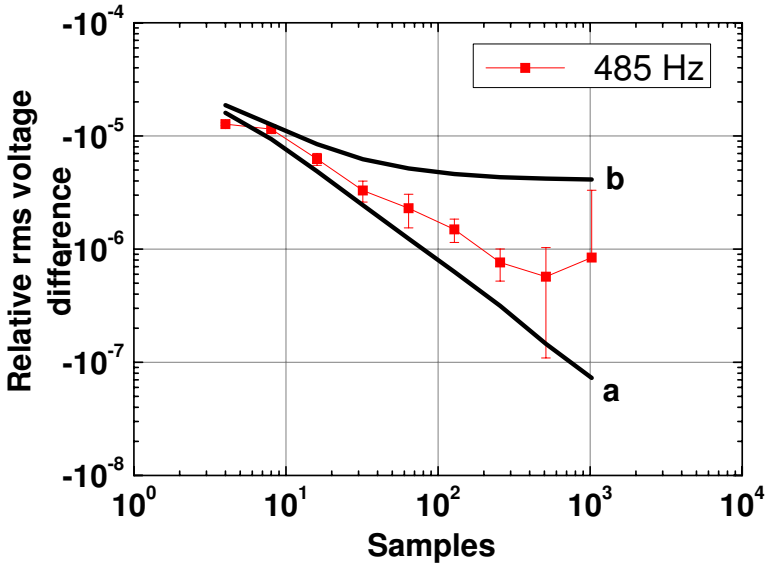

Figure 4.6: Difference from ideal of the rms value for different sample numbers. a) $t_{\mathrm{rise}} = t_{\mathrm{fall}}$, b) $t_{\mathrm{fall}} = t_{\mathrm{rise}}/1.2$. Measurements made at 485 Hz with different samples per period are indicated with the squares.

the frequency makes the step width smaller and the slope increases. The step center, i.e. $I_{\mathrm{trim}} = 0$, also shows a linear increase of the transfer difference with frequency. This increase becomes clearly visible above 520 Hz.

The influence of the number of samples per period used for the stepwise approximation of the waveform was studied at a very close frequency, 485 Hz. Figure 4.6 shows both the model predictions and the experimental data. The rms value of a waveform is related to its integral over one period and is thus related to the area enclosed in that time. As the transients from the presented model are slower than the arbitrarily short ones in the ideal waveform, the area is smaller and the rms value lower.

If $t_{\mathrm{rise}} = t_{\mathrm{fall}}$, the error in the rms value due to transients for a given time constant can be reduced by increasing the number of samples N_{Samples} [8]. On the other hand, if $t_{\mathrm{rise}} = t_{\mathrm{fall}} + \Delta t$, the influence of N_{Samples} on the rms value of the synthesized waveform decreases as N_{Samples} increases. Figure 4.6 shows these two predictions from the presented model for a stepwise approximated sine wave of 485 Hz. The case where $t_{\mathrm{rise}} = t_{\mathrm{fall}} = 50$ ns is marked as **a** and $t_{\mathrm{fall}} = t_{\mathrm{rise}}/1.2$ is marked as **b** in figure 4.6. The data points show measurements performed with the PMJTC and $N_{\mathrm{Samples}} = 4, 8, 16, \ldots 1024$ and clearly lie between these two curves. Therefore, it can be assigned that $t_{\mathrm{fall}} \approx t_{\mathrm{rise}}/1.1$ on the present system for transients estimation.

It should be noted that the ratio $t_{\text{rise}}/t_{\text{fall}}$ becomes exactly 1, see 2.14 and 2.17, if the array is biased to the center of the Josephson step and the width of the zero and first order steps is the same, $I_{0H} = \frac{1}{2}(I_{1H} - I_{1L})$.

Chapter 5

Josephson Impedance bridges

5.1 The Josephson Two-Terminal-Pair Bridge (J2T)

The basis of the concept is to setup a bridge using two Josephson systems each driving a synthesized AC wave to each of the standard resistors [Jinni-4]. Next, a null detector is placed in the center of the bridge, it is hence quantifying the difference in the resistor values. Balancing the bridge to reach a complete symmetry will require the two Josephson Waveform Synthesizers (JWSs) generate voltage waveforms with the necessary phase difference to null the voltage difference at the middle point between the impedances. A small residual voltage will be measured by the null detector.

A simplified circuit diagram is shown in figure 5.1 showing that the natural way of obtaining the difference in value between the resistors is hence

$$\frac{V_1}{V_2} = \frac{Z_1}{Z_2} \tag{5.1}$$

5.1.1 Experimental Setup

Figure 5.2 shows a complete schematics of the coaxial setup. The two JWSs, each comprised of a programmable Josephson array, its microwave source and bias electronics, are connected in series with the pair of impedance standards as described before. The 50-Ω resistors in the schematics are for canceling reflections caused by the load when the system is not impedance matched. The array, together with the 50-Ω resistors, is in liquid Helium temperature of 4 K and pressure in the dewars is stabilized to 102.0 kPa ± 50 Pa.

As discussed previously, the rms voltage of the waveform generated by the JWS depends on the exact shape of the transients, which in turn are influenced by parameters like the

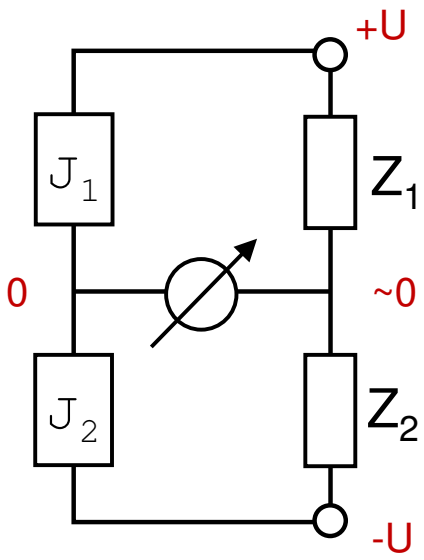

Figure 5.1: Simplified schematic diagram of the two-terminal-pair Josephson impedance bridge.

bias current used or the microwave power [Jinni-2]. The fundamental component of a square wave is chosen for measurement as it has the lowest dependence on the transients [14; 38].

The two 10-kΩ resistors represent the standard resistors constructed for this work. In this setup, only the voltage leads of the standards will be used and the current leads were left as open circuit.

5.1.2 Measurement Procedure

In the measurements, the Josephson waveform amplitudes and the phase difference between them are adjusted such that the null detector reading is close to zero. Using programmable Josephson arrays in the JWSs implies no or little increase in the uncertainty when the impedance ratio being measured is different from 1:1 by more than a few parts in 10^{-6}. If the resistances of the two JWSs, R_{J1} and R_{J2}, all the additional impedances — such as the contact resistance of the connectors and the cable resistances, both of the inner and outer conductors — were precisely known, a single measurement would allow one to calculate the ratio of the resistances R_1 and R_2 seen at terminals T_1 and T_2 (figure 5.2) based on the calculable Josephson voltages. However, R_{J1} and R_{J2} and the additional resistances are known only approximately. The problem can be alleviated by performing two sets of measurements, as shown in figure 5.3, in which the position of R_1 and R_2 relative to the sources is swapped. The *forward* configuration means that JWS1 and JWS2 set the voltages

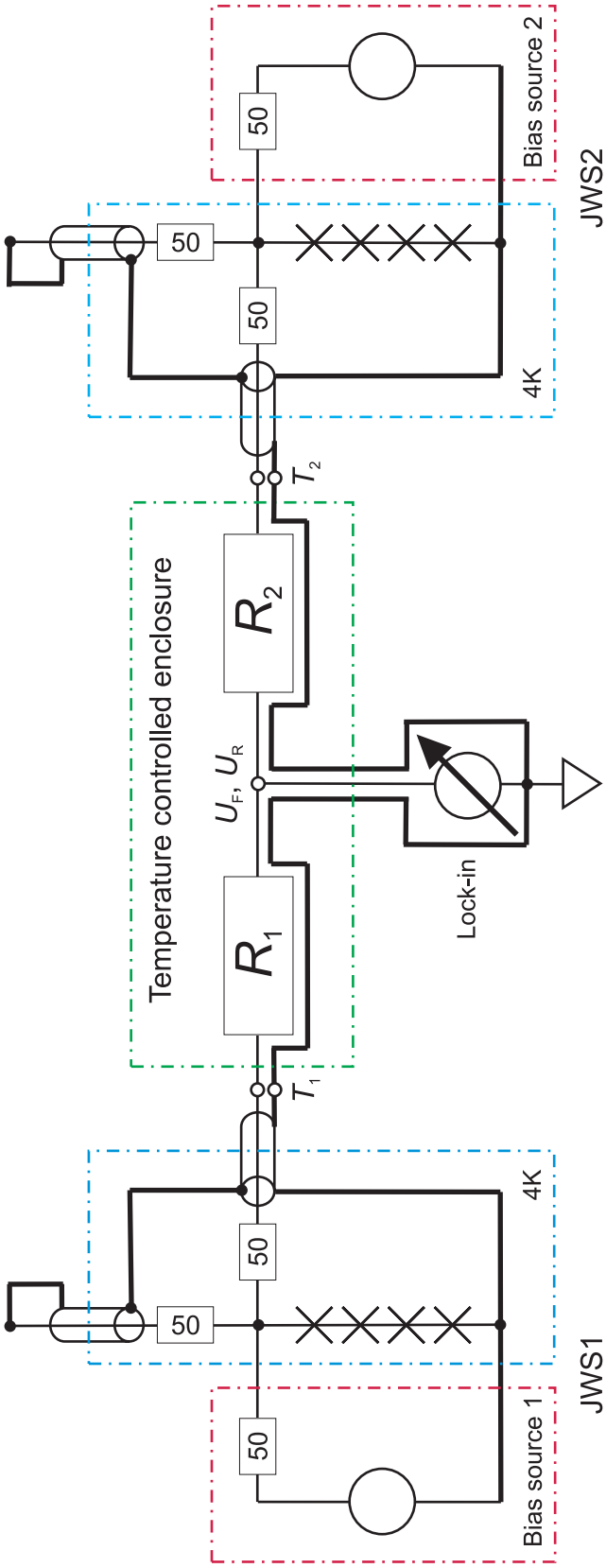

Figure 5.2: Schematic diagram of two Josephson waveform synthesizers connected with the lock-in amplifier and the pair of resistance standards. (The thick black lines are drawn to indicate outer conductors of the system)

across R_1 and R_2, respectively. In the *reverse* configuration, JWS1 sets the voltage across R_2 and JWS2, across R_1. In order to differentiate between the different amplitudes programmed in the two configurations, the voltages in the *reverse* configuration are denoted with a prime symbol (’). With this method the additional resistances and R_{J1} and R_{J2} need not be known exactly; only their difference must be stable during the whole measurement for best accuracy.

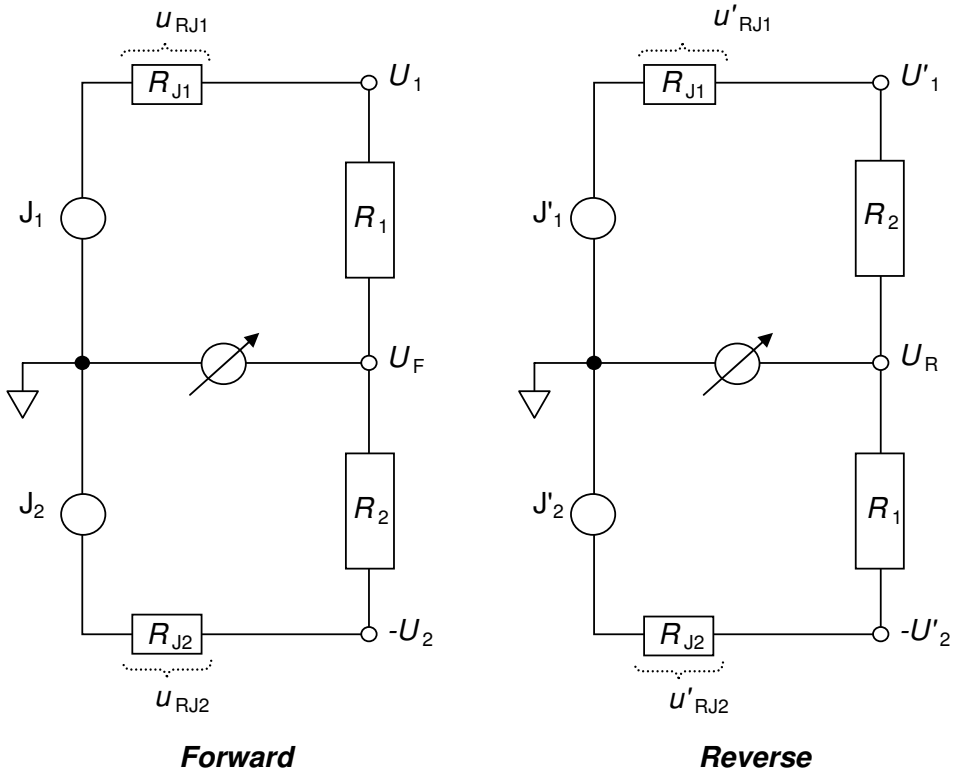

Figure 5.3: Simplified circuit diagram illustrating the *forward* and *reverse* bridge configurations with reversal of the resistors R_1 and R_2. The voltages are referred in equation 5.2.

5.1.2.1 Bridge Balancing Procedure

As with conventional two-terminal-pair impedance bridges, the balanced condition is satisfied when the voltage difference measured at the input of the null detector is zero. The top part of figure 5.4 shows this difference signal in the J2T bridge when the two JWSs are programmed to exactly the same voltage and phase. This trace was acquired when measuring a 10-kHz signal using the AC amplifier of a digital lock-in amplifier connected as shown in figure 5.2. In order to null the voltage difference during the quantized state of the JWS outputs, the microwave frequency used in one of them is tuned (lower part in figure 5.4). The area under

the transients is minimized by adjusting the relative phase between the two JWSs outputs. It should be noted at this point that the 80-kHz bandwidth of the AC amplifier considerably widens the transients. These transients are in quadrature phase relative to the signal and their contribution to the results is negligible as shown later.

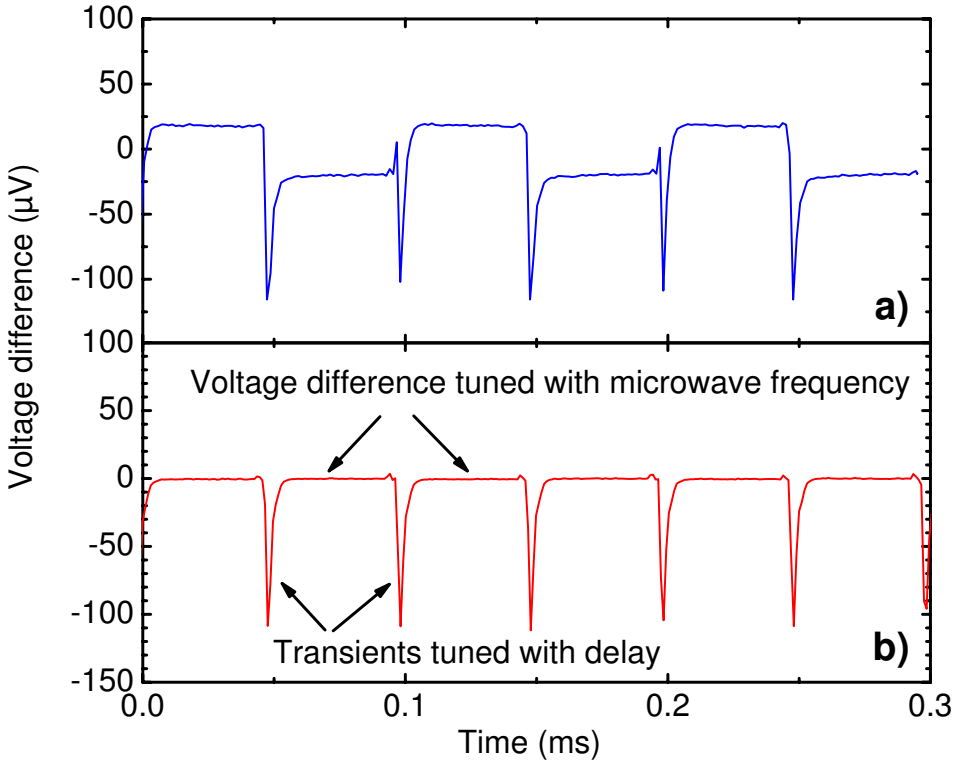

Figure 5.4: Voltage difference at the input of the lock-in amplifier: a) before balancing, b) after both voltage and phase are balanced.

The two resistors R_1 and R_2 have very similar values – they deviate just by 2.6 $\mu\Omega/\Omega$ according to a measurement performed with a conventional bridge. The relative difference between the two 50-Ω SMD-resistors (R_{J1} and R_{J2}) is ten times larger. Balancing the bridge requires a change in the microwave frequency of one JWS from e.g. 70.2785 GHz to 70.2790 GHz when the setup is reversed. As previously described, this can be done under software control. Neither the 1 mA widths of the voltage steps of the array nor their absolute position in bias current changes significantly between the different frequencies. The voltage at the lock-in amplifier is typically kept smaller than 2 μV to reduce linearity errors.

Figure 5.5 shows the lock-in measurements for the magnitude of the voltage difference in dependence of the delay between the Josephson bias sources for a 250-Hz rectangular waveform. The minimum magnitude corresponds to the two waveforms being time-aligned

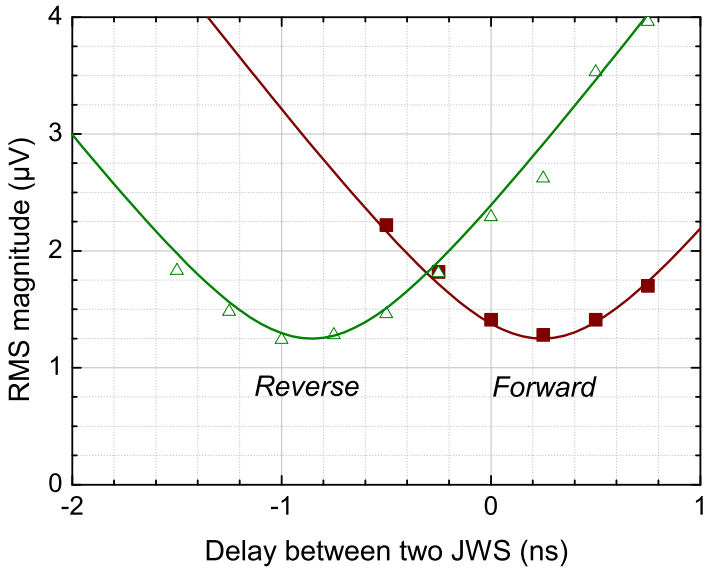

Figure 5.5: Magnitude of the voltage difference at the input of the lock-in as a function of the delay between the two JWSs for both *forward* (■) and *reverse* (△) measurements at a signal frequency of 250 Hz. The absolute delay values are arbitrary.

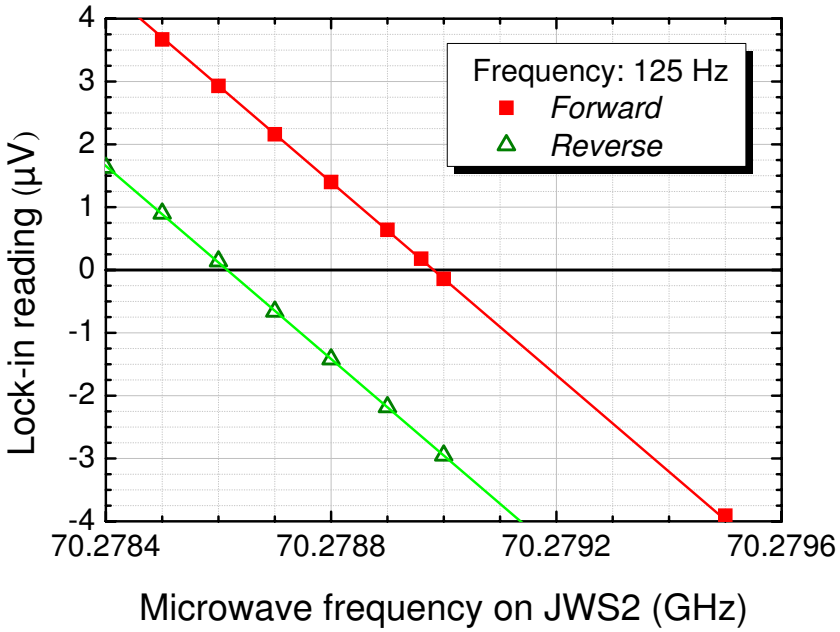

Figure 5.6: *Forward* and *reverse* voltage differences at 125 Hz when the amplitude of one JWS is changed by altering its microwave frequency.

at the input of the lock-in. The difference between the fits for the curves in the *reverse* and *forward* configurations results in a difference in parasitic capacitance between the two resistors and their associated cables of 110 fF ± 5 fF. This value is in excellent agreement with the 115 fF measured with a conventional bridge.

The effect of varying the microwave frequency on the lock-in amplifier magnitude reading is shown in figure 5.6. The relative phase between the two JWSs was set for minimum voltage (see figure 5.5). As expected, the lock-in readings depend linearly on the microwave frequency.

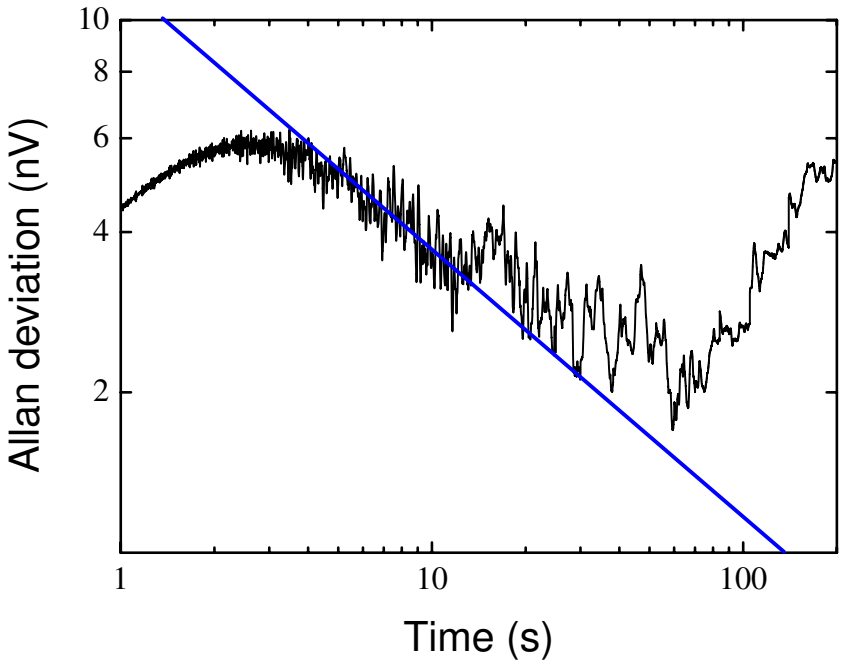

Figure 5.7: Allan deviation analysis for measurement made with the lock-in amplifier every 20 ms. The dependence for white noise is shown as a visual aid.

5.1.2.2 Lock-in Amplifier Settings

In order to optimize the timing of the experiment an Allan deviation analysis is performed [39]. Figure 5.7 shows the result for 40000 measurement points with 20 ms sample time, thus covering 13 minutes. The graph demonstrates that measurements follow well the white noise regime between 5 s and 60 s. For times larger than 60 s a steep increase is visible which indicates a drift within the system. A measuring time of 15 s with 1 s time constant is chosen for the data presented in this paper. This short measuring time is within the

white noise regime and sufficient in this low noise setup to achieve a relative uncertainty of ≈ 4 nV/1.2 V $\approx 3{\times}10^{-9}$.

This short measurement time allows making a complete frequency sweep in the *forward* or *reverse* configuration within 10 minutes. The variations in the additional impedances in the setup is thus kept small. The ratio of the resistances was measured at 18 frequencies between 25 Hz and 10 kHz. The frequency is changed automatically by the computer program by changing the repetition frequency of the pulse generator used to trigger the JWSs. Each frequency change requires a waiting time of 10 seconds to let the system settle and the lock-in to stabilize.

5.1.2.3 Test for Quantization

The signature of a quantum standard is that the output remains constant when one or more parameters are modified. For DC voltage, the current used to bias the junctions in a programmable Josephson array to a constant voltage step can be trimmed over a certain range without any changes in output voltage. For AC waveforms generated with a JWS, the transients between quantized voltages change as a result of the different bias current [Jinni-2]. The resulting variation relevant for the measurements, the amplitude of the fundamental of the square wave generated, depends quadratically on the ratio between the duration of the transient and the period of the square wave generated [14; 38]. At a signal frequency of 10 kHz, a resolution of 50 nV for the lock-in corresponds to a variation in the duration of the transients below 23 ns.

Figure 5.8 shows the in-phase component (X) and the quadrature component (Y) at the input of the lock-in amplifier at a frequency of 10 kHz when the bias current is trimmed relative to the center of the step. In addition, the in-phase component when the phase setting of the lock-in is modified by 0.3 degrees (X') is also shown to illustrate the sensitivity of this adjustment. In both cases, the in-phase component changes slope sharply for bias trim currents of -0.4 mA and +0.4 mA. The total cable capacitance between the middle point of the resistors and the input of the lock-in introduces a phase shift into the measurements. It has been found that the phase setting for a flat in-phase component varies linearly with frequency by 6 degrees between 25 Hz and 10 kHz. This matches the dependence expected for cable capacitance of 140 pF. The lock-in phase settings for flat X components are measured at different signal frequencies and subsequently used when changing the signal frequency for the impedance ratio measurements.

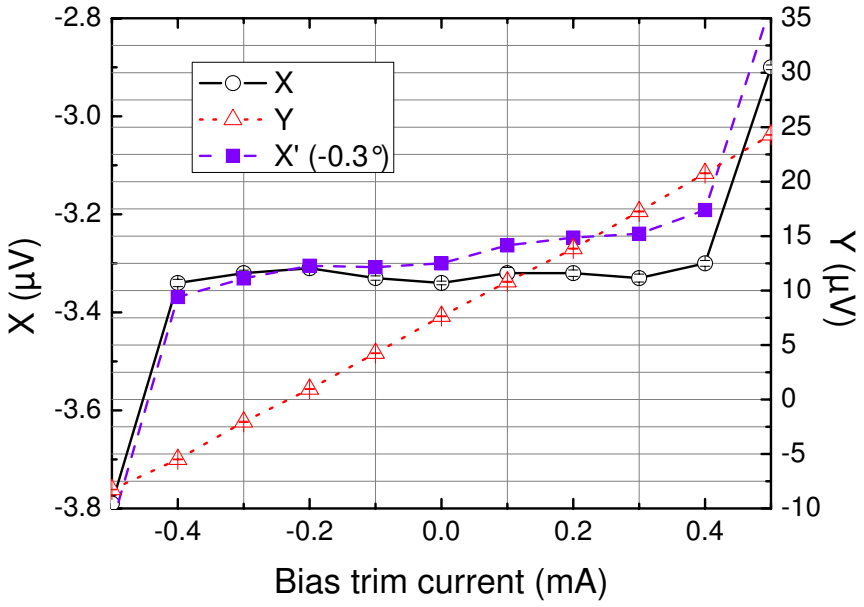

Figure 5.8: In-phase (X) and quadrature (Y) voltages at the input of the lock-in amplifier as a function of the bias trim current for a signal frequency of 10 kHz. Note that the vertical scales are different by a factor of 10.

5.1.2.4 Calculations

In summary, the measurement procedure works in several steps as follows. First, the highest signal frequency is set and the two Josephson systems are connected to the two resistors and set to generate opposite voltage waveforms. The JWS amplitudes are chosen in a way such that the in-phase component at the lock-in is zero to balance the bridge. Then the phase between the two waveforms is optimized i.e. the magnitude of the signal at the input of the lock-in is minimized (figure 5.5). Finally, the phase setting of the lock-in amplifier is adjusted such that the in-phase component is insensitive to changes in the Josephson array bias current inside the constant voltage step.

For a pair of *forward* and *reverse* measurements balanced according to this procedure and using the voltages depicted in figure 5.3, the resistance ratio is:

$$G = \frac{R_1 - R_2}{R_2} = \frac{1}{2}\left[2 - \left(\frac{U_2}{U_1} + \frac{U_\mathrm{F}}{U_1} + \frac{U_\mathrm{F}}{U_2}\right) - \left(\frac{U_1'}{U_2'} - \frac{U_\mathrm{R}}{U_1'} - \frac{U_\mathrm{R}}{U_2'}\right)\right] , \tag{5.2}$$

where

$$U_\mathrm{i} = U_\mathrm{Ji} - U_\mathrm{RJi} , \tag{5.3}$$

$$U_\mathrm{Ji} = \frac{4}{\pi} \cdot \frac{f_\mathrm{i}}{K_{\mathrm{J}-90}} \cdot 8192 \quad (\mathrm{i} = 1, 2). \tag{5.4}$$

U_{J1} and U_{J2} represent the amplitude of the fundamental generated by the Josephson systems JWS1 and JWS2, respectively. U_{RJ1} and U_{RJ2} denote the voltages across the 50-Ω resistors connected to the voltage lines for the reflection compensation connection. The unprimed and primed symbols correspond to the *forward* and *reverse* connections, respectively. The lock-in voltage for the *forward* connection is U_F and U_R for the *reverse* one.

When performing measurements at different frequencies, one configuration is started at the highest frequency and balance the bridge as just described. As the frequency is changed, only the phase setting in the lock-in is modified according to the values previously established from scans of the bias current at different signal frequencies. After measuring at all the frequencies desired, the configuration is changed, e.g. from *forward* to *reverse,* and the bridge is balanced again at the highest frequency.

5.1.3 Uncertainty Analysis

5.1.3.1 Mathematical Model

The ratio readout G from the system is obtained from the equation 5.2, in addition that the voltage across the 50-Ω U_{RJ1} is,

$$U_{RJ1} = \frac{R_a \cdot (U_{J1} + U_{J2})}{R_1 + R_2 + R_a + R_b} \tag{5.5}$$

$$x = U_F - U_R = \frac{(U_{J1} + U_{J2}) \cdot (R_1 + R_a) - (U_{J1} + U_{J2}) \cdot (R_2 + R_a)}{R_1 + R_2 + R_a + R_b} \tag{5.6}$$

Major sources of Type-B uncertainties in the measurement include

R_1: Value of resistor 1

R_2: Value of resistor 2

U_{J1}: Voltages generated by the Josephson systems JWS1

U_{J2}: Voltages generated by the Josephson systems JWS2

U_F: Lock in voltage at *forward* connection

U_R: Lock in voltage at *reverse* connection

U_{RJ1}: Voltage across the 50-Ω resistors connected to the voltage lines of JWS1

U_{RJ2}: Voltage across the 50-Ω resistors connected to the voltage lines of JWS2

R_a: the 50-Ω resistors connected to the voltage lines of JWS1

R_b: the 50-Ω resistors connected to the voltage lines of JWS2

5.1.3.2 Uncertainty Equation

The combined standard uncertainty of the measured ratio $u_c(G)$ is given as the positive square root of the combined variance $u_c^2(G)$[40], which is given by:

$$u_c^2(G) = \sum_{i=1}^{N} \left(\frac{\delta G}{\delta x_i}\right)^2 u^2(x_i) \tag{5.7}$$

The combined variance can be viewed as a sum of terms, each of which represents the estimated variance associated with the output estimate generated by the estimated variance associated with each input estimate. The combined standard uncertainty can hence be expressed as a series of sensitivity coefficients,

$$\begin{aligned} u_c^2(G) \;=\; & \left(\frac{\delta G}{\delta R_1}\right)^2 u^2(R_1) + \left(\frac{\delta G}{\delta R_2}\right)^2 u^2(R_2) + \left(\frac{\delta G}{\delta U_{J1}}\right)^2 u^2(U_{J1}) + \left(\frac{\delta G}{\delta U_{J2}}\right)^2 u^2(U_{J2}) \\ & + \left(\frac{\delta G}{\delta U_F}\right)^2 u^2(U_F) + \left(\frac{\delta G}{\delta U_R}\right)^2 u^2(U_R) + \left(\frac{\delta G}{\delta u_{RJ1}}\right)^2 u^2(u_{RJ1}) + \left(\frac{\delta G}{\delta u_{RJ2}}\right)^2 u^2(u_{RJ2}) \\ & + \left(\frac{\delta G}{\delta r_a}\right)^2 u^2(r_a) + \left(\frac{\delta G}{\delta r_b}\right)^2 u^2(r_b) \end{aligned}$$

where the sensitive coefficients are

$c_1 = \frac{\delta G}{\delta R_1} = \frac{\delta G}{\delta R_2} = \frac{\delta G}{\delta r_b} = \frac{U_R - U_F}{U_J(R_{all} - 2r_a)} - \frac{R_{all}(U_R - U_F)}{U_J(R_{all} - 2r_a)^2}$

$c_2 = \frac{\delta G}{\delta U_{J1}} = \frac{\delta G}{\delta U_{J2}} = -\frac{R_{all}(U_R - U_F)}{U_J{}^2(R_{all} - 2r_a)}$

$c_3 = \frac{\delta G}{\delta U_R} = -\frac{\delta G}{\delta U_F} = -\frac{R_{all}}{U_J(R_{all} - 2r_a)}$

$c_4 = \frac{\delta G}{\delta R_a} = \frac{\delta G}{\delta R_b} = \frac{U_R - U_F}{U_J(R_{all} - 2r_a)} + \frac{R_{all}(U_R - U_F)}{U_J(R_{all} - 2r_a)^2}$

A detailed report is generated by the GUM Workbench [41] is presented in Appendix A.3. It gives an example of uncertainty calculations made for this setup using typical values and the resulting expanded uncertainty of ± 21 x 10^{-9} (k = 2).

5.1.4 Results and Discussion

Measurements from the J2T bridge for frequencies from 25 Hz to 10 kHz are compared with measurements made with the conventional bridge in figure 5.9. The dashed line is a polynomial fit to the values measured by the J2T bridge, and is just to guide the eye. Each measurement result from the J2T bridge is the average of 4 sets of *forward-reverse* pairs having a type-A uncertainty ($k = 1$) of about 2 parts in 10^{-8} for frequencies from 25 Hz to 6 kHz. Each point for either configuration is the average of the lock-in readings over 15 s. Just the two highest frequencies, 8 kHz and 10 kHz, show an increased uncertainty. This is because the influence of the transients is more pronounced.

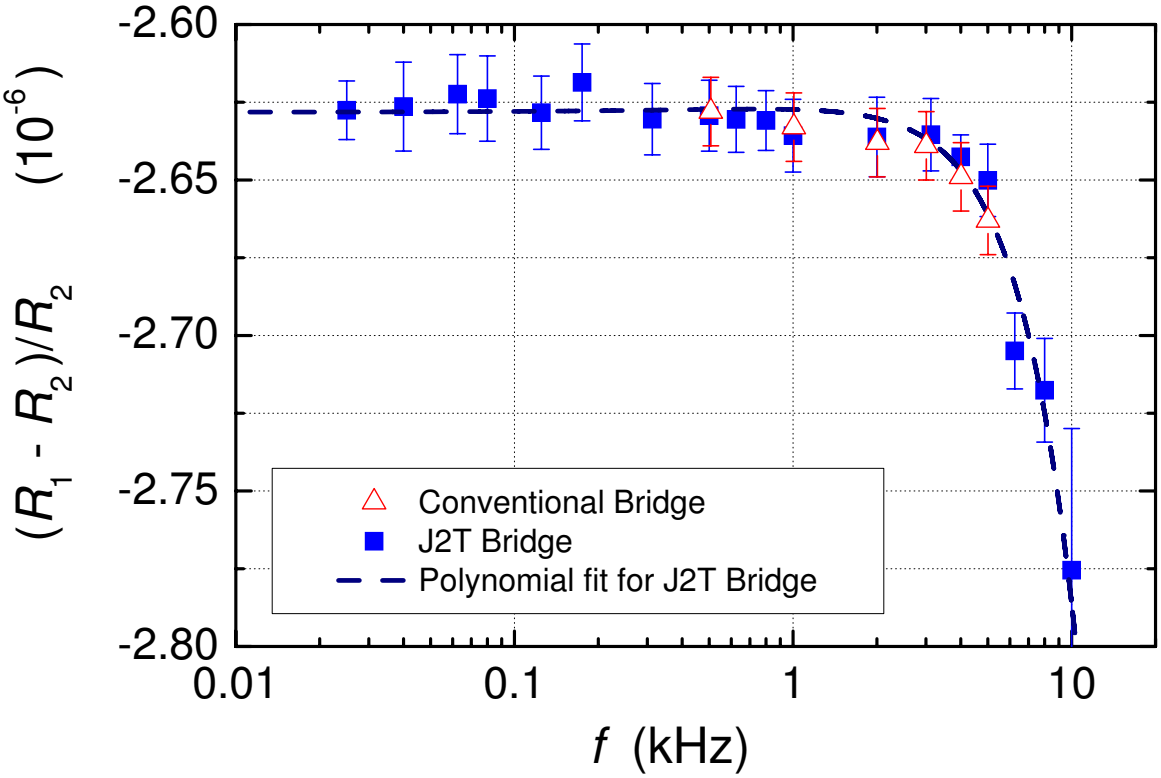

Figure 5.9: Resistance ratio measurements from the J2T bridge (■) and from a conventional two-terminal-pair impedance ratio bridge (△).

The J2T bridge measurements show very good agreement with the measurements made with the conventional bridge, depicted in figure 5.9 as open triangles. We can clearly conclude that at frequencies below 5 kHz the results from the J2T bridge match those of the conventional bridge to a few parts in 10^{-8}. Another advantage of the J2T bridge is given by its capability to compare different impedances with effective phase angles of any degree.

Large phase differences between the voltages applied to the impedances can be programmed into the bias sources in the JWSs and fine tuned with the programmable delay in steps as small as 250 ps.

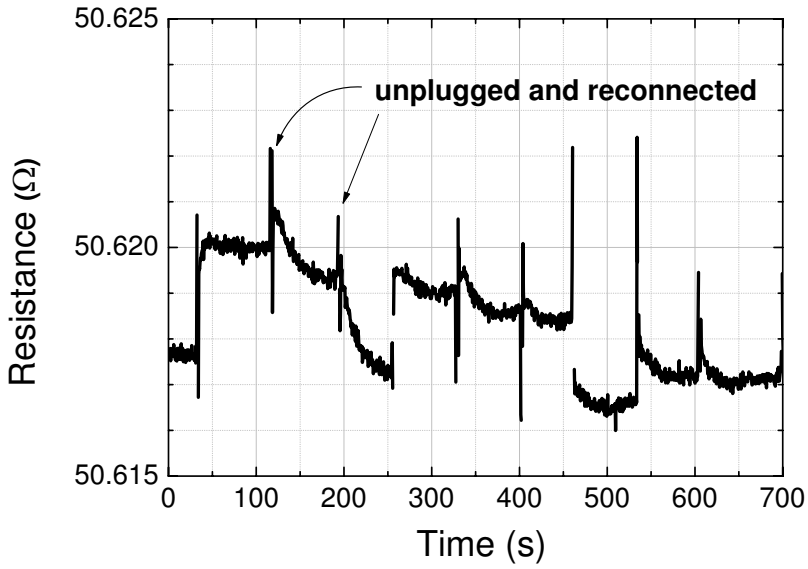

Figure 5.10: Time series for measurements of the 50 Ω output resistance of a JWS with its Josephson array unbiased. The spikes are due to the BPO connectors being unplugged and reconnected.

The accuracy of any kind of two-terminal-pair impedance measurement system is limited by the reproducibility and the stability of the contact resistance and cable impedances in the measurement circuit. To evaluate the influence of the contact resistance, the output resistance of one Josephson system was measured. This was done with an Agilent 3458A digital voltmeter in two-terminal-pair mode and the Josephson array on the zero step. The BPO connector was unplugged and directly re-connected. Figure 5.10 shows a time series of these measurements. The spikes indicate the connecting cycles. Apart from the sudden changes in resistance of up to 2 mΩ, the average resistance change for sets of 10 disconnections and re-connections was 1 mΩ. As it can be calculated, a 2 mΩ difference in the resistance of the systems results in a 0.1 $\mu\Omega/\Omega$ change in the measured resistance ratio.

5.2 The Four-Terminal-Pair Setups

A four-terminal measurement is the technique that uses separate pairs of current-carrying and voltage-sensing wires for making more accurate measurements than two-terminal systems. When the condition is met such that there are no currents flowing through the voltage leads, the resistance value can be defined at the point of connection between the voltage and the current lines on both sides of the resistor. At the same time, electrical and magnetic interferences are eliminated and the problem of contact resistance that is seen in the two-terminal setup does not exist in the four-terminal setup.

5.2.1 Potential Comparison Circuit

The four-terminal-pair configuration of this section is a setup of a potential comparison circuit making use of the AC Quantum Voltmeter (ac-QVM)[Jinni-5]. The ac-QVM is an instrument for measuring AC waveforms by comparing them to a Josephson waveform. It has been successfully tested and first measurements at the ± 2.4 p-p V level give an uncertainty of 5 x 10^{-8} (k = 1) [12]. The concept is to use a sampling digital voltmeter connected together with a Josephson Waveform Synthesizer (JWS) to measure the difference between the generated waveform and the source waveform. For simplicity, we will name this circuit configuration as J4T-PCC for Josephson four-terminal-pair potential comparison circuit.

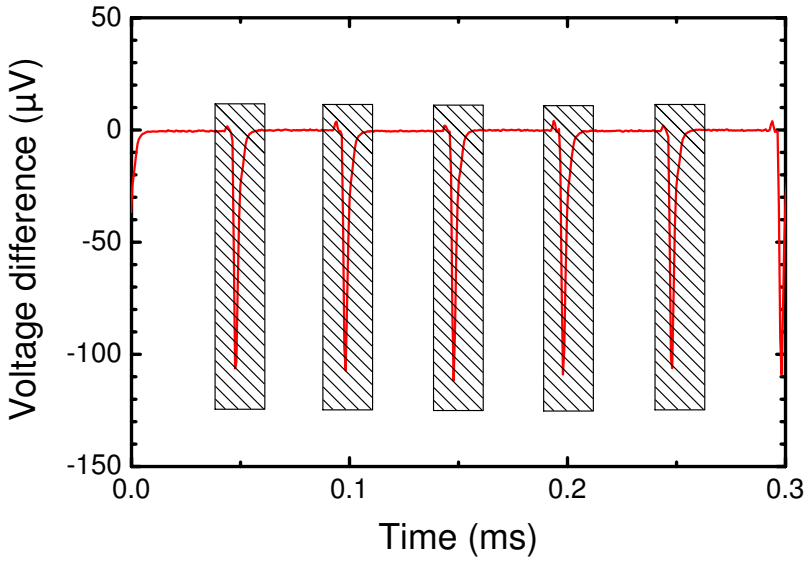

Figure 5.11: Shaded portions of the synthesized waveform are not measured in the sampling method. Measurements only taking into account the parts where voltage steps are quantized.

By using the sampling techniques with digital voltmeters, the uncertainties due to transients can be avoided. Sampling allows measurements to be made in slices of a 'window'. Instead of measuring the whole waveform as it is done with the lock-in amplifier, a sampling digital voltmeter (DVM) such as the Agilent 3458A collects data within a designated period of a given waveform. This method can be simply demonstrated in figure 5.11 where only the windows of the quantized waveform are measured. The greyed out area containing unwanted transients of a synthesized waveform can be completely ignored.

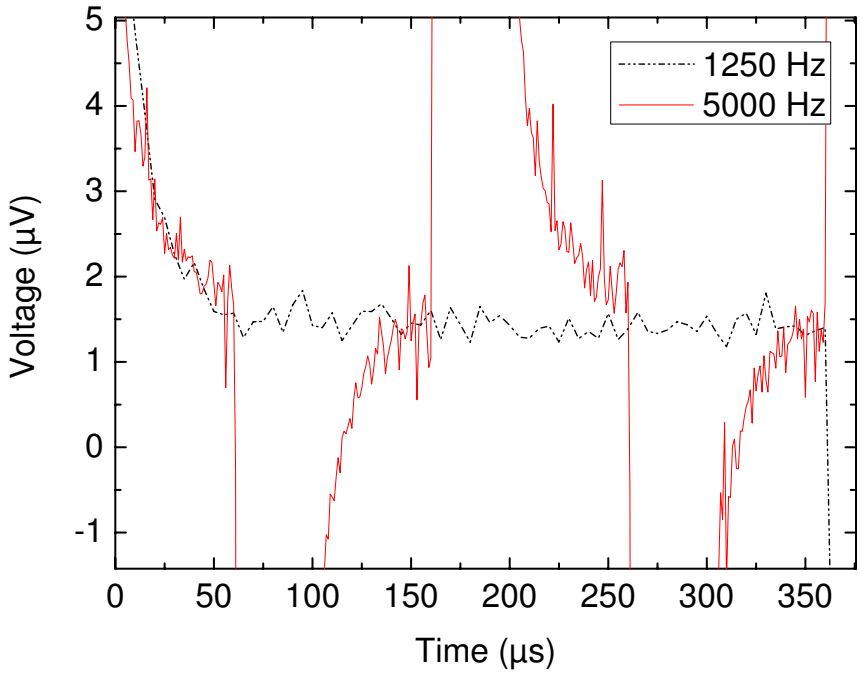

Figure 5.12: Time trace of a 5 kHz waveform compared to a 1250 Hz waveform showing the width of measurable quantized steps reduces as sample frequency increases.

The downside of this method is that the window that accommodates quantized step measurements gets smaller and smaller as the sample frequency increases. As shown in figure 5.12, the time trace of a 5 kHz sample waveform is compared to the 1250 Hz waveform. The 5 kHz waveform has a narrow measurable width of an aperture time that is less than 20 μs as opposed to the 1250 Hz waveform that has a wide integratable time of more than 200 μs. The large settling time of the transients is caused by the relaxation of the sampling DVM its input filters are charged by the transients [42]. It has a capped sample frequency of 6 kHz in this present setup. This can be improved if the settling time of transients seen by the sampling DVM is shortened or by having a faster A-D converter with high precision.

5.2.1.1 Characterizing Amplifiers

The major component of the ac-QVM is the null-detector. Since the voltage differences measured are kept to as low as 1 μV, measurements are dominated by the null-detector noise [43]. To overcome this fact, small voltage levels can be amplified. An amplifier with a gain of 100 is used as described in [44].

To test the performance of the amplifier, it is placed between two synchronized JWSs. Figure 5.13 shows a measurement of a synchronized 4-sample Josephson waveform in the frequency range from 80 Hz to 4 kHz [Jinni-6]. Measurements are made on the voltage difference between positive and negative 1-V steps, and the voltage difference between the 0-V steps of the 4-sample waveform. Measurements made at the 0-V steps act as a check for determining the presence of unwanted offset levels that is adding voltage to the null-detector.

Overloading of the pre-amplifier is avoided by tuning the programmable delay unit to prevent large voltages output from the waveform transients.

The measurements show very small voltage differences of less than 10 nV. This means that the relative uncertainty is less than 1 part in 10^8, and that is an improvement by a factor of five at the 1-V level in uncertainty and frequency range [12].

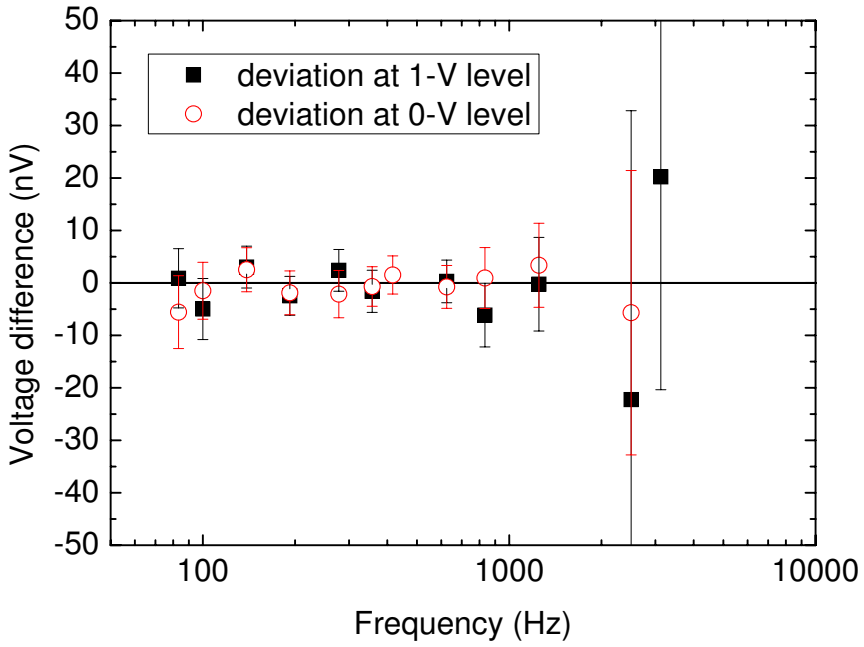

Figure 5.13: Measurement of two Josephson 4-samples waveforms using a differential pre-amplifier[Jinni-6].

5.2.1.2 Experimental Setup and Procedure

Figure 5.14 shows the schematic used for this setup. The JWS_{source} depicted in the left acts as a source for driving the two standard resistors, whereas the JWS_{meter} on the right plays the role as a meter for balancing a null on the detector. The JWS_{source} in this setup configuration uses a stacked Josephson array of 2.4 V [45] and generates 1.2 Vp-p to each of the resistors. The null-detector connected in between the resistors measures the difference voltage between the source and the JWS_{meter}.

Similar to the J2T bridge, Josephson waveform amplitudes and the phase difference between the two systems are adjusted such that the null detector reading is close to zero. Subsequently, a series of measurement parameters are given to the sampling voltmeter for collecting readings in a different frequency range. Next, the JWS_{meter} is shifted together with the sampling DVM to the connections of resistor R_2. The same procedure is followed.

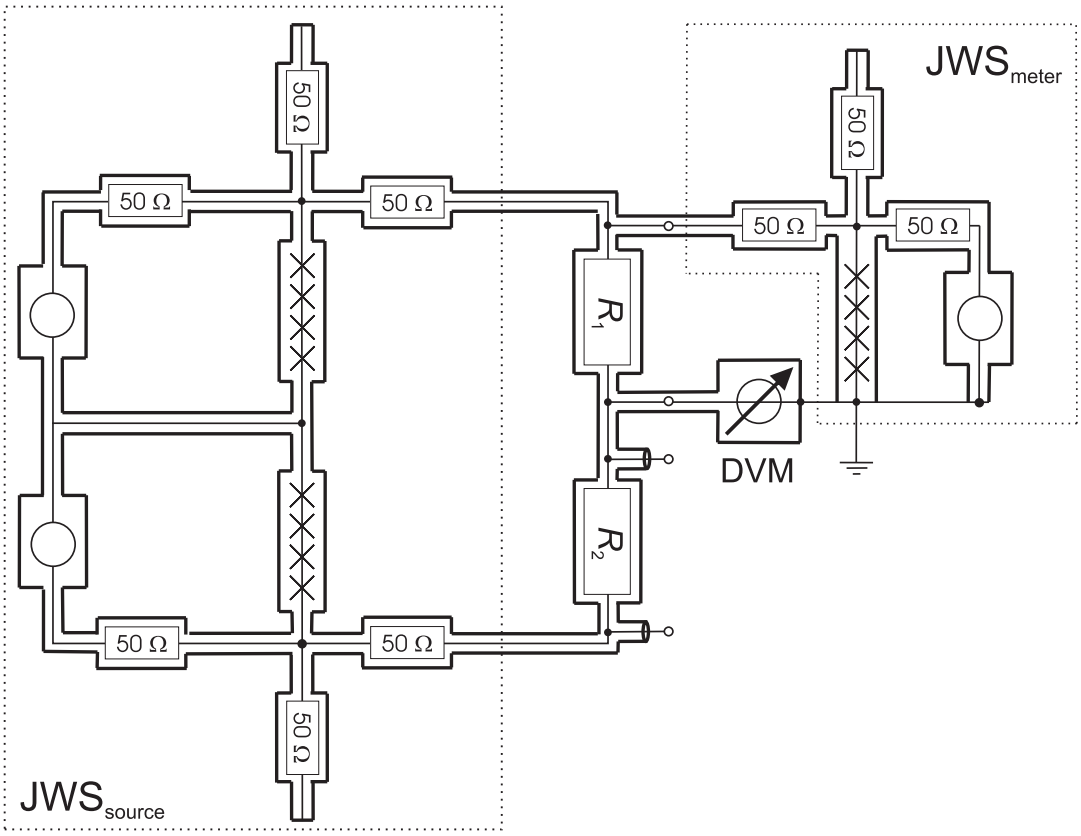

Figure 5.14: Schematic diagram of the 4-terminal-pair measurement setup using ac-QVM as a potential comparison circuit.

Frequency (Hz)	Aperture time (μs)
20	5000
40	2000
139	1000
400	700
1250	200
2500	100
4000	20
6250	10

Table 5.1: Table of the measuring frequency and its corresponding integration time used.

The resistance ratios between the standards can be calculated as [6]:

$$\frac{R_1 - R_2}{R_2} = \frac{U_{\text{meter}} - U_{\text{reading}}}{U'_{\text{meter}} - U'_{\text{reading}}} - 1 \tag{5.8}$$

where U_{meter} is the voltage generated by $\text{JWS}_{\text{meter}}$ and U_{reading} is the voltage measured by the sampling DVM at the connection to R_1. The same goes for the configuration when the ac-QVM is switched to the connection of R_2, and the difference is denoted with a prime symbol (').

Each measured frequency is set with a different aperture time that is programmed for measurement mining as given in table 5.1, since different frequencies have different width of measurable window. The highest frequency of 6250 Hz has reached a minimum measurement window time of 10 μs integration time since it is limited by the large settling transients time that is experienced by the voltmeter input filter (as shown in figure 5.12). Each measurement is made to a duration of 2 minutes.

5.2.1.3 Results and Discussion

Figure 5.15 shows the preliminary measurement results of the J4T-PCC, as compared with measurement results from the J2T. Each result point per frequency is an average of 10 measurements, of which each single measurement is the reading of the sampling DVM over 120 s. Type-A uncertainties (k = 1) for frequencies below 1 kHz are less than 1 part in 10^{-8}, which demonstrates a successful outcome for the sampling technique.

The setup as a potential comparison circuit is very good for measuring at low frequencies since the accuracy of the sampling-method increases greatly due to longer measurable time on the quantized step. Unlike the J2T bridge, the J4T-PCC does not suffer from the inconsistencies of contact resistance. However, the limit of this setup is restricted to a highest measurable frequency of 6 kHz due to the lack of effective measurement window.

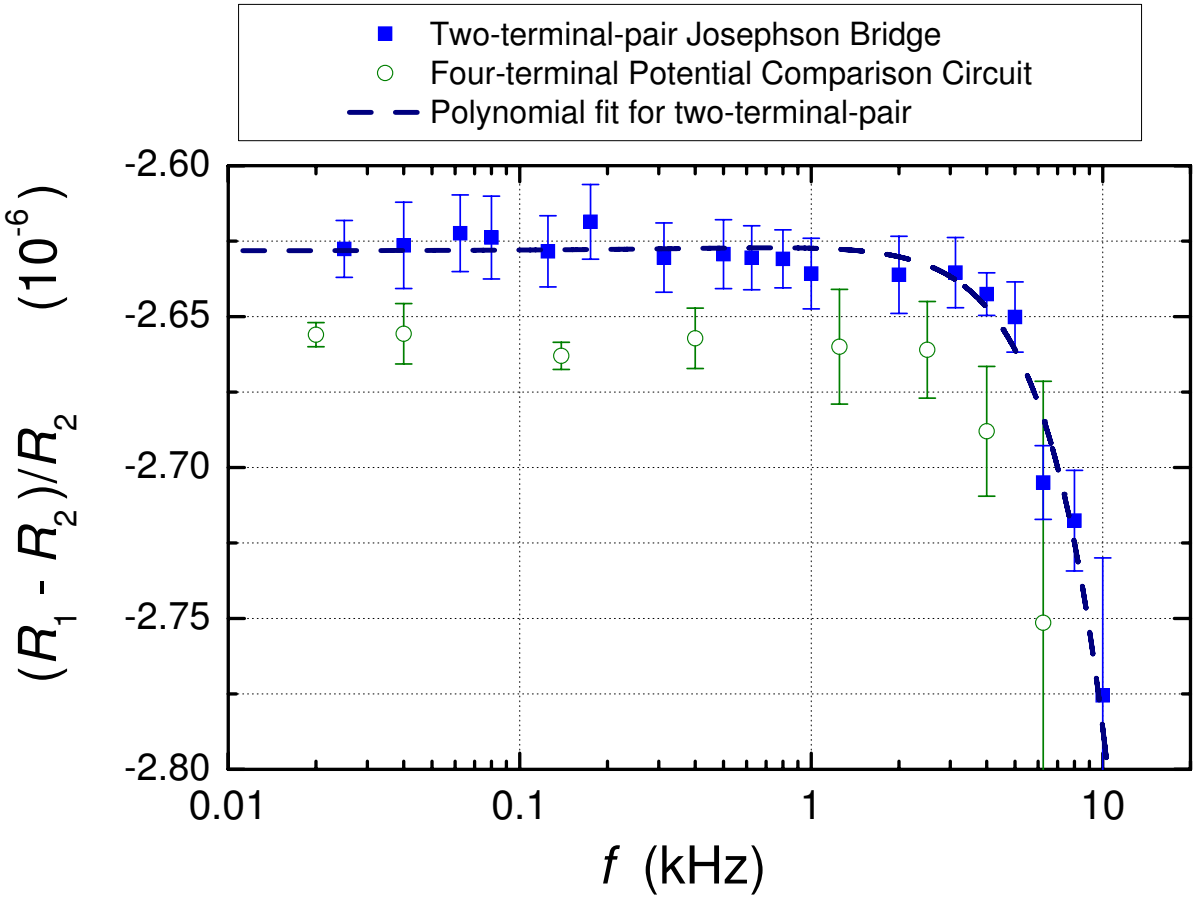

Figure 5.15: Preliminary measurement results of the Josephson four-terminal-pair potential comparison circuit, as compared with measurement results from the Josephson two-terminal-pair impedance bridge.

The slightly lower shift of the sampling measurements of 3 x 10^{-8} as compared to measurements made by the J2T bridge equates to a change of 0.3 mΩ. The value is reasonable to account for contact resistances seen in the J2T bridge.

However, this is not an impedance measurement as it does not measures the complex component. An impedance measurement would be given by:

$$Z = \frac{U}{I} = R \cdot (1 + j\omega RC + \omega^2 LC) \tag{5.9}$$

As the J4T-PCC setup has disregarded the measurements from the transients, the last two components $j\omega RC$ and $\omega^2 LC$ are not measured. Therefore, the results shown above accounts only to the real component of the resistors and this setup lacks the ability to perform phase measurements.

5.2.2 Outlook - Coaxial Circuit

For making a true impedance four-terminal-pair measurement, the whole waveform has to be measured with a lock-in amplifier. One concept is to have a completely symmetrical coaxial bridge circuit. As shown in figure 5.16 each resistor on the coaxial setup has four leads connecting to it, two current leads and two voltage leads, hence fulfilling the 4-terminal definition of a resistor. The current-carrying leads of the resistors are the horizontal lines across the resistors whereas the voltage leads are the vertical lines from the resistors. The two systems JWS1 and JWS2 comprise of the same components as mentioned in the section of the J2T bridge where they consist of the bias electronics and the 50-Ω resistors for canceling reflections.

The schematics show that the JWS drives the resistors on their current leads with full array (1.2 V p-p) and runs half of the array (0.6 V p-p) on the voltage-sensing leads of the resistors. A switch (Switch 1, Switch 3) is connected to one end of the voltage-sensing leads of a resistor, and an adjustable 10 kΩ is connected to the current lead on the same end of the resistor.

This part of the bridge is balanced by tuning the value of the 10 kΩ adjustable resistor such that the detector (lock-in amplifier) registers no change when opening or closing switch 1. At this point, there will be no current flowing through the voltage lead that is indicated in the schematic diagram ($i = 0$). The same goes for balancing the loop on the side of JWS2 using Switch 3.

In the center of the bridge, the approach is applied similarly by using a Kelvin Double Bridge [46]. A switch (Switch 2) is installed between the current leads of both resistors and a pair of 100 Ω is connected in the loop to the lock-in amplifier. This section of the bridge

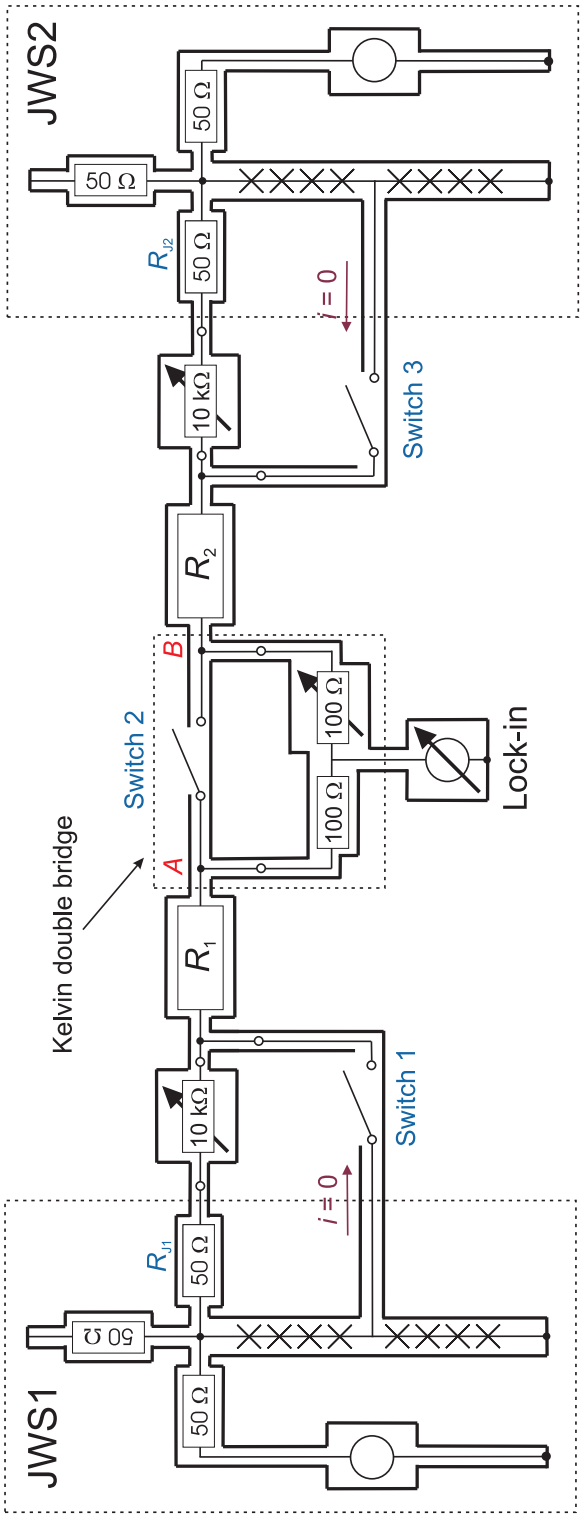

Figure 5.16: Schematic diagram of the 4-terminal-pair potential comparison circuit using the lock-in amplifier.

balances in the same manner as above: the adjustable 100 Ω is tuned to a value in which opening or closing switch 2 does not cause a change in the lock-in reading. When this is achieved, the potential difference between points A and B can be described as being truly zero.

Since both Josephson arrays are set in two different dewars and attached to two different cryo-probes, there are dissimilarities in the resistances of the outer-conducting cables on the probes. It is measured that the resistance of outer conductors on the two cryo-probes are about 500 mΩ. Assuming a 2% difference on the resistances of the cryo-probes together with a 50 μA current flowing in the system, results in: 10 mΩ x 50 μA / 0.6 V = 833 nV/V, which is a huge difference comparing to the uncertainty that is aimed to be at nanovolt level. This problem can be solved in two ways: either by ensuring no differences or low resistance on the cryo-probes; or by performing a reversal of swapping the two JWSs, as identical to the reversal procedure for the J2T bridge.

When all balancing conditions are met, the lock-in amplifier gives a value that is equivalent to U_F, or the measured voltage in a *forward* configuration. A following reversal is made and the bridge has to be re-balanced once more due to the differences in the 50-Ω resistors (R_{J1} and R_{J2}). Equations that are previously used to describe the J2T bridge likewise can be applied in this setup for calculations of the final resistors ratio.

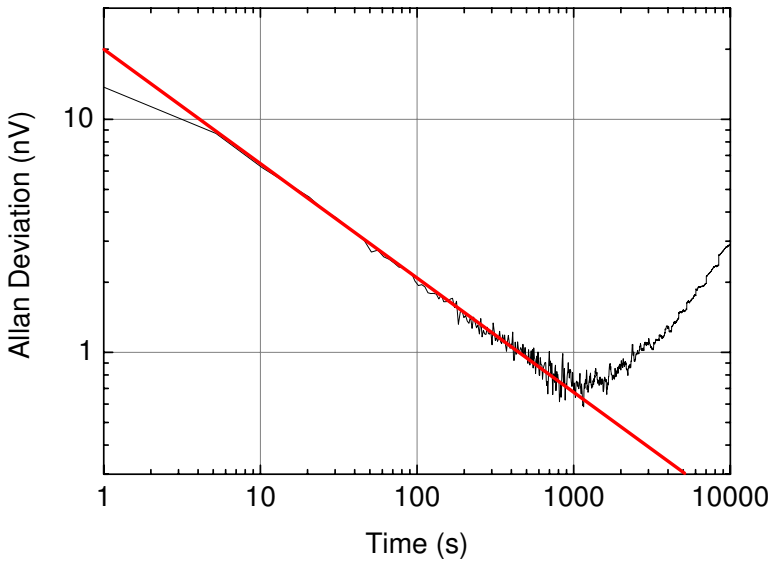

Figure 5.17: Allan deviation for measurements made on the 4-terminal-pair coaxial setup.

Preliminary Allan deviation of this setup shows promising results (figure 5.17). Measurements were made with 200,000 readings with 100 ms per sample. The graph indicates that

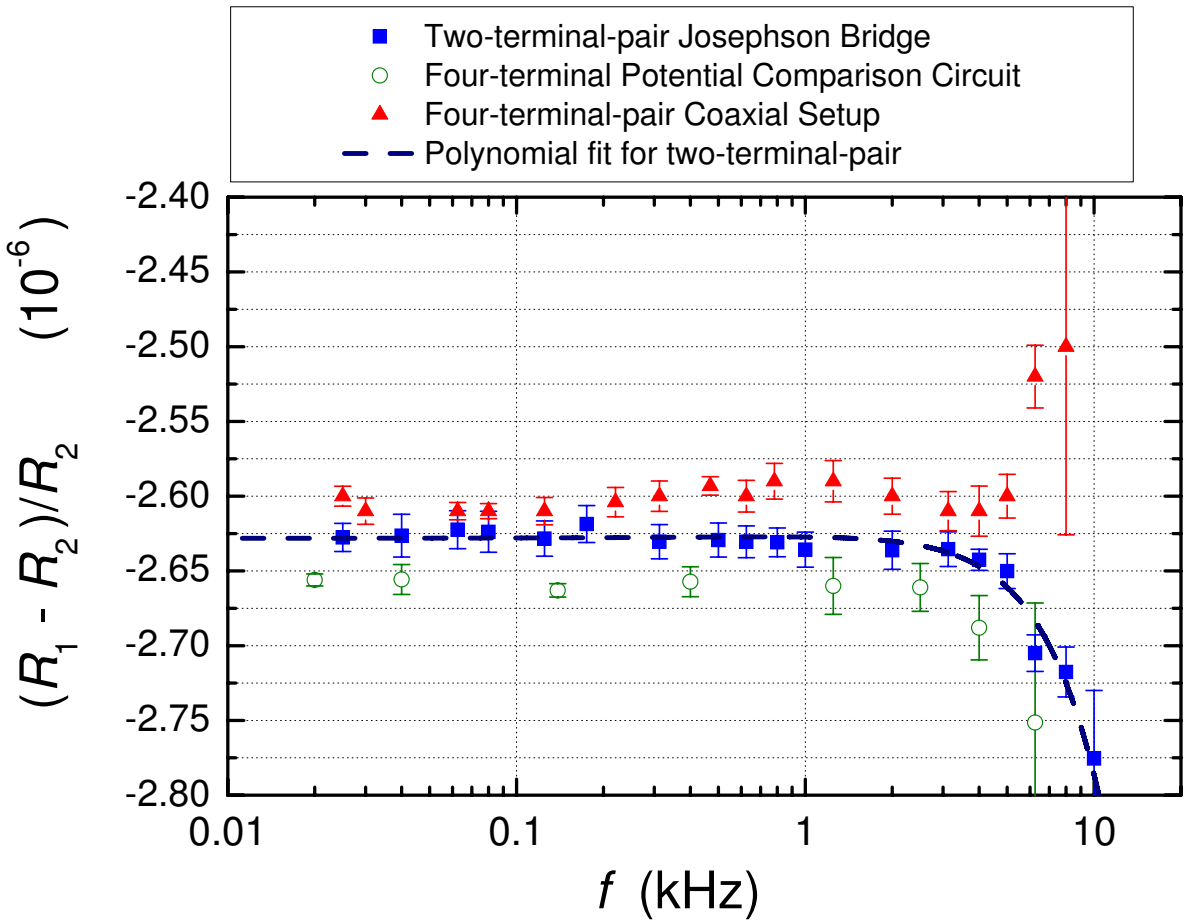

Figure 5.18: Preliminary results of the four-terminal-pair coaxial circuit compared with results shown in previous graphs of the J2T bridge and the J4T-PCC. Error bars show type-A uncertainty.

measurements follow the white noise well into 1000 s or 17 min with a Allan deviation value of less than 1 nV. This is a strong proof that the setup is very stable and it exhibits great potential to achieve measurement accuracies of at least a factor of 10 better than the J2T bridge (refer to figure 5.7), even though manual balancing of the bridge may be unavoidable.

The preliminary results of the four-terminal-pair coaxial circuit show agreement to the J4T-PCC setup to about 6 parts in 10^8 for frequencies below 5 kHz, while they clearly reveal a systematic error within the setup (figure 5.18). The type-A uncertainties of frequencies below 5 kHz are on average at 10^{-9} levels (k = 1). The unexpected change in frequency dependence at high frequencies may be due to the fact that the transients were affecting the setup largely when balancing the bridge.

Another reason is that due to the mismatched resistance in the cryo-probe cables, the

setup does not have equal and opposite currents flowing through the system. Current equalizers are commonly installed on a conventional bridge to achieve equal and opposite currents flowing between the inner and outer conductors. However they cannot be used on this setup as they corrupt the transients extensively. Hence this may cause the setup to collect electrical or magnetic interferences from the environment contributing to the systematic error seen in the graph.

One of the challenges faced is that when opening the switches for balancing, there are large amounts of reflections experienced by the system. Transients of the generated waveforms become at least 10 times larger and hence cause a big error contribution in measuring high frequencies. This may be the reason for the inconsistency seen in the frequency dependence that is determined by the bridge.

The investigation of the four-terminal-pair-coaxial configuration remains a preliminary examination so far. It has the potential of type-A uncertainties to reach lower levels than 10^{-9} as soon as the systematic errors are figured out. Further observation will be required such as the bridge sensitivity, pin-pointing the sources of system offsets and minimizing the resistance differences between the outer conductors of the two JWSs.

5.3 Outlook for Future Josephson bridges

The method of using Josephson voltage sources as impedance bridges is presently uncharted and there will be great perspectives ahead. First and foremost, additional development can be made on impedances with unlike phase angle differences, for example by comparing a capacitance and resistance standard.

Subsequently, larger unconventional ratios could be tested even to levels of 10:1 or more. This would be especially favorable in the dissemination of the quantum hall resistance of 12,906 kΩ to conventional impedance standards that have values in multiples of 10.

Chapter 6

Conclusion

An innovative concept for impedance bridges based on programmable Josephson quantum voltage standards has been developed and tested. It has been demonstrated that the measurements made by the programmable Josephson impedance bridges are comparable to conventional bridges, notwithstanding many other additional benefits.

The uncertainty of the rms value in the stepwise synthesized Josephson waveforms, used in Josephson bridges, depends on errors contributed by the transients. A simple model for describing the influence of bias current and array parameters on the transients has been presented. It has been confirmed experimentally with thermal converter measurements that rms measurements at 1 kHz have a type-A uncertainty of $1{\cdot}10^{-6}$ [Jinni-2]. Measurement procedures that use the fundamental component of a Josephson generated rectangular waveform show the smallest dependence on variations of the transients. Quantization at up to 10 kHz has been confirmed by varying the bias current of the Josephson arrays resulting in constant resistance ratios within the measurement resolution of a few parts in 10^8 [14; 38].

The Josephson 2-terminal-pair setup (J2T) demonstrated that impedance measurements made between two 10 kΩ resistances reach an uncertainty of a few parts in 10^8 for frequencies below 6 kHz, which is comparable to conventional impedance bridges. In addition, the measurement of 110 fF ± 5 fF for the differences in parasitic capacitances of the resistance standards is determined and it is in accurate agreement with the 115 fF measured using the quadrature component of a conventional impedance bridge.

For 4-terminal Josephson bridges, the potential comparison setup determines the resistance ratios to a few parts in 10^{-8} and a factor of 3 better for frequencies below 1 kHz. As the potential comparison setup is based on voltmeter sampling methods, it does not measure the complex components between the resistors.

The 4-terminal-pair coaxial circuit setup covers the ability to evaluate the complex impedance of the resistance standards. It shows an agreement with the results from the

potential comparison setup to about 6 parts in 10^8, while more investigations have to be made to understand the systematic errors within the deviation between the two different 4-terminal setups. The coaxial circuit setup has been shown to be very stable at a type-A uncertainty below 10^{-9}, so that once the problems are solved, there is great potential of reaching very good overall uncertainties.

The measurement results in this work prove that the Josephson bridge system (both 2-terminal and 4-terminal setups) can match the uncertainty of conventional impedance bridge setups. In addition, impedance measurements can be made at arbitrary frequencies in a wide-band range from DC to 10 kHz, as compared to conventional bridges with fixed frequencies restricting to the multiples of 500 Hz to 10 kHz. Furthermore, both J2T bridge and the 4-terminal-pair potential comparison circuit setup will allow automated operation, whereas conventional automated impedance ratio bridges commonly loose accuracy due to the performance limitation of electromechanical relays in the circuit. Measurements procedures are able to be easily executed by a pre-determined program sweeping through the desired frequency and phase ranges.

In summary, it has been proven that the Josephson impedance bridges are capable of performing impedance ratios measurements as accurately as conventional bridges. It has also been demonstrated that the capabilities of the Josephson bridge system exceeded conventional bridges largely due to its ability to measure in a broad bandwidth and its scope for complete automation without loss of uncertainty. Although the new Josephson impedance bridge technique, pioneered by this work, is still in its early development state, it has proven its potential for applied and fundamental ac impedance metrology. Recently, it was shown that the Farad can be traced to the Ohm via the ac quantum Hall effect accurately by using conventional impedance bridges [47]. In the future, the new Josephson bridge technique may for instance provide an independent way of realizing this link.

References

[1] B. P. Kibble and G. H. Rayner, *Coaxial AC Bridges*. Adam Hilger Ltd, Bristol, 1984.

[2] B. J. S. Neil M Zimmerman and Y. Wang, "An upper bound to the frequency dependence of the cryogenic vacuum-gap capacitor," *Metrologia*, vol. 43, pp. 383–388, 2006.

[3] B. Wood and S. Solve, "A review of Josephson comparison results," *Metrologia*, vol. 46, pp. R13–R20, 2009.

[4] P. Warnecke, J. Niemeyer, F.-W. Dünschede, L. Grimm, G. Weimann, and W. Schlapp, "High-precision resistance ratio measurements by means of a novel Josephson potentiometer," *IEEE Trans. Instrum. Meas.*, vol. 36, pp. 249–251, 1987.

[5] C. Hamilton, C. Burroughs, and R. Kautz, "Josephson D/A converter with fundamental accuracy," *IEEE Trans. Instrum. Meas.*, vol. 44, pp. 223–225, 1995.

[6] R. Behr, T. Funck, B. Schumacher, and P. Warnecke, "Measuring resistance standards in terms of the quantized Hall resistance with a dual Josephson voltage standard using SINIS Josephson arrays," *IEEE Trans. Instrum. Meas.*, vol. 52, pp. 521–523, Apr. 2003.

[7] C. A. Hamilton, C. J. Burroughs, S. P. Benz, and J. R. Kinard, "AC Josephson Voltage Standard: Progress Report," *IEEE Trans. Instrum. Meas.*, vol. 46, pp. 224–228, Apr. 1997.

[8] J. M. Williams, P. Kleinschmidt, T. J. B. M. Janssen, P. Patel, R. Behr, F. Müller, and J. Kohlmann, "Synthesis of precision AC waveforms using a SINIS Josephson junction array," *CPEM 2002 Conf. Digest*, pp. 434–435, Jun. 2002.

[9] J. Nissilä, K. Ojasalo, A. Kemppinen, A. Manninen, J. Hassel, P. Helist, and H. Seppä, "Development of a quantum ac voltage standard based on externally shunted Josephson arrays," *CPEM Conf. Dig.*, pp. 158–159, 2004.

[10] J. Nissilä, A. Kemppinen, K. Ojasalo, J. Hassel, A. Manninen, P. Helistö, and H. Seppä, "Realization of a square-wave voltage with externally-shunted SIS Josephson junction arrays for a quantum AC voltage standard," *IEEE Trans. Instrum. Meas.*, vol. 54, pp. 636–640, Apr. 2005.

[11] R. Behr, J. M. Williams, P. Patel, T. J. B. M. Janssen, T. Funck, and M. Klonz, "Synthesis of precision waveforms using a SINIS Josephson junction array," *IEEE Trans. Instrum. Meas.*, vol. 54, pp. 612–615, Apr. 2005.

[12] R. Behr, L. Palafox, G. Ramm, H. Moser, and J. Melcher, "Direct comparison of Josephson waveforms using an AC Quantum Voltmeter," *IEEE Trans. Instrum. Meas.*, vol. 56, pp. 235–238, Apr. 2007.

[13] A. Rüfenacht, C. J. Burroughs, S. P. Benz, P. D. Dresselhaus, B. C. Waltrip, and T. L. Nelson, "Precision differential sampling measurements of low-frequency synthesized sine waves with an AC programmable Josephson voltage standard," *IEEE Trans. Instrum. Meas.*, vol. 58, pp. 809–815, Apr. 2009.

[14] B. Jeanneret, F. Overney, A. Rüfenacht, and J. Nissilä, "Strong attenuation of the transients effect in square waves synthesized with a programmable Josephson voltage standard," *to be published in IEEE Trans. Instrum. Meas.*, 2009.

[15] C. Burroughs, A. Rüfenacht, S. Benz, P. Dresselhaus, B. Waltrip, and T. Nelson, "Error and Transient Analysis of Stepwise-Approximated Sinewaves Generated by Programmable Josephson Voltage Standards," *IEEE Trans. Instrum. Meas*, vol. 57, pp. 1322–1329, 2008.

[16] B. D. Josephson, "The discovery of tunnelling supercurrents," *Rev. Mod. Phys.*, vol. 46, pp. 251–254, 1974.

[17] L. Essen and J. V. L. Parry, "An Atomic Standard of Frequency and Time Interval: A Caesium Resonator," *Nature*, vol. 176, pp. 280–282, 1955.

[18] S. Shapiro, "Josephson Currents in Superconducting Tunneling: The Effect of Microwaves and Other Observations," *IEEE Trans. Instrum. Meas.*, vol. 11, pp. 80–82, 1963.

[19] J. Niemeyer, "Josephson voltage standards," *Handbook of Applied Superconductivity, B. Seeber (Ed.)*, pp. 1813–1834, 1998.

[20] W. C. Stewart, "Current-voltage characteristics of Josephson junction," *Appl. Phys. Lett.*, vol. 12, p. 277280, 1968.

[21] D. E. McCumber, "Effect of ac Impedance on dc Voltage-Current Characteristics of Superconductor Weak-Link Junctions," *Journal of Applied Physics*, vol. 39, pp. 3113–3118, 1968.

[22] R. Behr, F. Müller, and J. Kohlmann, "Josephson junction arrays for voltage standards," *Studies of Josephson junction arrays*, vol. 40, pp. 155–184, 2002.

[23] J. Clarke, "The proximity effect between superconducting and normal thin films in zero field," *Journal de Physique*, vol. 29, pp. C 2–3, 1968.

[24] D. Bracken and W. O. Hamilton, "Comparison of Microwave-Induced Constant-Voltage Steps in Pb and Sn Josephson Junctions," *Phys. Rev. B*, vol. 6, pp. 2603–2609, 1972.

[25] R. M. Macfarlane, R. M. Shelby, and R. L. Shoemaker, "Ultrahigh-Resolution Spectroscopy: Photon Echoes in YAlO3: Pr3+ and LaF3: Pr3+," *Phys. Rev. Lett.*, vol. 43, pp. 1726–1730, 1979.

[26] J. H. Hinken, J. Niemeyer, and R. L. Kautz, "Superconducting MMICs with 1474 Josephson Junctions Providing Standard Voltages up to 1.2 Volt," *Microwave Conference, 1984. 14th European*, pp. 761–766, 1984.

[27] F. L. Lloyd, C. A. Hamilton, J. A. Beall, D. Go, R. H. Ono, and R. E. Harris, "IA Josephson Array Voltage Standard at 10 V," *IEEE Electron Device Lett.*, vol. EDL-8, pp. 449–450, 1987.

[28] R. Pöpel, "The Josephson Effect and Voltage Standards," *Metrologia*, vol. 29, pp. 153–174, 1992.

[29] C. Hamilton, C. Burroughs, and R. Kautz, "Stable 1 volt programmable voltage standard," *Appl. Phys. Lett.*, vol. 71, pp. 1866–1868, 1997.

[30] J. Kohlmann, F. Müller, P. Gutmann, R. Pöpel, L. Grimm, F. W. Dunschede, W. Meier, and J. Niemeyer, "Improved 1 V and 10 V Josephson voltage standard arrays," *IEEE Trans. Appl. Supercond.*, vol. 7, pp. 3411–3414, Jun. 1997.

[31] http://www.jsquid.com, Jülicher Squid GmbH.

[32] R. Behr, L. Palafox, T. Funck, J. M. Williams, P. Patel, and A. Katkov, "Synthesis of precision calculable AC waveforms," *CPEM 2006 Conf. Digest*, pp. 440–441, Jul. 2006.

[33] S. P. Benz, P. D. Dresselhaus, C. J. Burroughs, and N. F. Bergren, "Precision measurements using a 300 mV Josephson arbitrary waveform synthesizer," *IEEE Trans. App. Superconductivity*, vol. 17, pp. 864–869, Jun. 2007.

[34] R. P. Landim, S. P. Benz, P. D. Dresselhaus, and C. J. Burroughs, "Systematic-Error Signals in the AC Josephson Voltage Standard: Measurement and Reduction," *IEEE Trans. Instrum. Meas.*, vol. 57, pp. 1215–1220, Jun. 2008.

[35] A. Katkov, R. Behr, and J. Lee, "Model for transient variation in stepwise synthesized Josephson sinewaves," *CPEM 2008 Conf. digest*, pp. 380–381, Jun. 2008.

[36] P. Kleinschmidt, P. Patel, J. M. Williams, and T. J. B. M. Janssen, "Investigation of binary Josephson arrays for arbitrary waveform synthesis," *Proc. Inst. Electr. Eng. - Sci. Meas. Technol.*, vol. 149, pp. 313–316, Nov. 2002.

[37] J. M. Williams, D. Henderson, P. Patel, R. Behr, and L. Palafox, "Achieving Sub-100-ns Switching of Programmable Josephson Arrays," *IEEE Trans. Instrum. Meas.*, vol. 56, pp. 651–654, Apr. 2007.

[38] J. Nissilä, A. Kemppinen, K. Ojasalo, J. Hassel, A. Manninen, P. Helistö, and H. Seppä, "Realization of a square-wave voltage with externally-shunted SIS Josephson junction arrays for a quantum AC voltage standard," *IEEE Trans. Instrum. Meas.*, vol. 54, pp. 636–640, Apr. 2005.

[39] T. J. Witt, "Using the Allan Variance and Power Spectral Density to Characterize DC Nanovoltmeters," *IEEE Trans. Instrum. Meas.*, vol. 50, pp. 445–448, Apr. 2001.

[40] I. O. for Standardization, *Guide to the Expression of Uncertainty in Measurement, GUM*, 1 Rue Varamb, Case Postale 56, CH 1221, Geneva, Switzerland.

[41] "Gum workbench," http://www.gum.dk/e-wb-home/gw_home.html.

[42] W. G. K. Ihlenfeld, E. Mohns, R. Behr, J. M. Williams, P. Patel, G. Ramm, and H. Bachmair, "Characterization of a High-Resolution Analog-to-Digital Converter With a Josephson AC Voltage Source," *IEEE Trans. Instrum. Meas.*, vol. 54, pp. 649–652, 2005.

[43] R. Behr, L. Palafox, and J. Kohlmann, "Improvements of the AC Quantum Voltmeter," *CPEM 2008 Conference Digest*, pp. 44–45, Jun. 2008.

[44] D. Henderson, K. M. Marshall, J. M. Williams, J. Pickering, and P. D. Patel, "A voltage source for low frequency AC waveforms with a quantum traceability to a Josephson array reference using sampling and feedback," *CPEM Conf. Dig.*, pp. 76–77, 2008.

[45] F. Müller, R. Behr, R. Wendisch, J. Kohlmann, D. Olaya, P. Dresselhaus, and S. P. Benz, "Arrays with double-stacked NbxSi1-x-barrier junctions for use in programmable Josephson voltage standards driven at 70 GHz," *12th International Superconductive Electronics Conference*, 2009.

[46] R. Hanke, "Precise Kelvin double bridge for measuring dissipation factors and capacitances up to 1 F," *IEEE Trans. Instrum. Meas.*, vol. 27, pp. 434–436, 1978.

[47] J. Schurr, V. Bürkel, and B. P. Kibble, "Realizing the Farad from two quantum Hall resistances," *Metrologia*, vol. 46, pp. 619–628, 2009.

List of Publications

Articles in International Journals and Reports:

Jinni-1: A. Katkov, R. Behr and J. Lee, "Model for transient variation in stepwise synthesized Josephson sinewaves", *CPEM 2008 Conf. digest*, pp. 380-381, Jun. 2008

Jinni-2: J. Lee, R. Behr, A. S. Katkov, L. Palafox, "Modeling and measuring error contributions in stepwise synthesized Josephson sine waves", *IEEE Trans. Instrum. Meas.*, Vol. 58, pp. 803-808, Apr. 2009

Jinni-3: J. Kohlmann, O.F. Kieler, R. Iuzzolino, J. Lee, R. Behr, B. Egeling and F. Muller, "Development and Investigation of SNS Josephson Arrays for the Josephson Arbitrary Waveform Synthesizer", *IEEE Trans. Instrum. Meas.*, vol. 58, no.4, pp. 797-802, Apr. 2009

Jinni-4: J. Lee, Jürgen Schurr, Jaani Nissilä, Luis Palafox, and Ralf Behr, "The Josephson Two-Terminal-Pair Impedance Bridge", *Metrologia*, vol. 47, no.4, pp. 453-459, Jul. 2010

Jinni-5: J. Lee, J. Schurr, J. Nissilä, L. Palafox and R. Behr, "Impedance Measurements with Programmable Josephson Systems", Conference on Precision Electromagnetic Measurements (CPEM) 2010, oral presentation

Jinni-6: R. Behr, D. Henderson, J. Williams, L. Palafox, J. Lee and J. Pickering, "Operation of the AC Quantum Voltmeter at Audio Frequencies", Conference on Precision Electromagnetic Measurements (CPEM) 2010, oral presentation

Presentations at International Conferences:

1. R. Behr, A. Katkov, J. Lee, L. Palafox, "Synthesis of ac waveforms using programmable Josephson arrays", EUROMET DC and Quantum and LF electrical metrology experts joint meeting, Espoo, 25-29, June, 2007 (Poster)
2. J. Lee, R. Behr, A. Katkov, and L. Palafox, "Uncertainty estimation for synthesizing sine waves with binary programmable Josephson standard arrays", International School of Quantum Metrology and Fundamental Constants, Centre de Physique des Houches, Les Houches, 1-12 Oct. 2007. (Poster)

3. A. Katkov R. Behr, and J. Lee, "Model for Transient Variation in Stepwise Synthesized Josephson Sinewaves", Conference on Precision Electromagnetic Measurements (CPEM), Broomfield, Colorado, USA, 8-13 Jun. 2008. (Poster)
4. L. X. Liu, S. W. Chua, J. Lee, Y. Zhou and C. A. Hamilton, "A Direct Comparison of Josephson Array Voltage Standards", Conference on Precision Electromagnetic Measurements (CPEM), Broomfield, Colorado, USA, 8-13 Jun. 2008. (Poster)
5. J. Lee, R. Behr, A. Katkov, and L. Palafox, "Error Contributions in Stepwise Synthesized Josephson Sine Waves", Conference on Precision Electromagnetic Measurements (CPEM), Broomfield, Colorado, USA, 8-13 Jun. 2008 (Oral Presentation)
6. J. Kohlmann, O.F. Kieler, R. Iuzzolino, J. Lee, R. Behr, B. Egeling and F. Müller, "Development and Investigation of SNS Josephson Arrays for the Josephson Arbitrary Waveform Synthesizer", Conference on Precision Electromagnetic Measurements (CPEM), Broomfield, Colorado, USA, 8-13 Jun. 2008 (Oral Presentation)
7. Y. Zhou, S.W.Chua, and J. Lee, "Enhancements of NMC's Josephson Array Voltage Standard System", Conference on Precision Electromagnetic Measurements (CPEM) 2010, accepted for poster presentation

Awards:

- CPEM 2008 Early Career Advancement Program Bursary Awardee (previously known as Young Scienctist Award)

Appendix A

Appendix

A.1 Binary Josephson Array Bias Source

Specifications

Waveform points	32,768 max
Amplitude resolution	15 array bits or 65,535 levels on 15 bit Arrays
Waveform memory	512k x 16 bit Static Random Access
Output current	5 mA Bipolar
Current driver resolution	14 bits
Settling time	20 ns on 50 Ohm load
Output compliance	$\pm$ 2 V
Front Panel connectors	15 SMBs (current outputs), 2 pin ADC input, 3 Optical Fibre connectors
Synchronized to external 10 MHz	TTL compatible or optical input
Computer interface	National Instruments PCI-6503
Power requirements	24 V dc, 5 A maximum
4U Standard Eurorack dimensions	480 mm x 180 mm x 430 mm (W:H:D) approx
Weight	6 kg approx

A.2 System Controlling Software

Description of the different layers used in the Bias and System controlling software

Layer	Name	Description	Remark
7	GUI	User Interface (UI) layer	Part of this layer contains the system setup wizards;
6	Interface	UI to system interface layer	Wizards would not remotely controllable since direct access to hardware required
5	Jo-voltage	Defines Jo-voltages and Jo-voltage patterns for the system;	This layer requires segment definitions (of junctions in each BinArray segment)
4	Bias	Calculates bias currents and bias current patterns	Requires array characteristics such as step widths, current bias at the center of the step
3	Source current	Converts required bias currents to source voltages and source voltage patterns; calculates timing data	Uses source-channel to segment mapping; needs output and lead resistance values
2	Source voltage	Uploads voltages and voltage patterns to the source; Initiates voltage pattern scans	Uses source voltage calibration data; part of this layer is a voltage source calibration wizard
1	Source raw	Writes raw amplitude and timing data to (and reads them back from) NPL source (treats the source as an uncalibrated m-channel, n-bit, D to A converter)	Uses instrument address to handle more than one source
0	Low level comm	Communication layer (optical ring, source register access, CIN or DLL-based)	

A.3 Uncertainty Budget for Two-terminal-pair Josephson Impedance Bridge

(continues on next page)

Uncertainty Budget for the Two-Terminal-Pair Josephson Impedance Bridge

Uncertainty budget related to the set up of the Two-Terminal-Pair Josephson Impedance Bridge measuring an impedance ratio at 1:1.

The bridge is set up using two Josephson Waveform Synthesizer (JWS), generating rectangular waveforms at a frequency ranging from 25 Hz to 10 kHz. The two standard resistors to be measured, 10-kΩ Vishay VHP202 resistors, are mounted in a temperature controlled enclosure which is stabilized to 29.95 °C within ± 1 mK. Measurements are made with a lock-in amplifier at the range of 5µV and at a gain of 50 dB in this case.

Model Equation:

$$R_r=0.5*(2-((U_{J2}-u_{RJ2})/(U_{J1}-u_{RJ1})+U_F/(U_{J1}-u_{RJ1})+U_F/(U_{J2}-u_{RJ2}))-((U_{J1}-u_{RJ1})/(U_{J2}-u_{RJ2})+U_R/(U_{J1}-u_{RJ1})+U_R/(U_{J2}-u_{RJ2})));$$

$$u_{RJ1}=R_a*(U_{J1}+U_{J2})/(R_a+R_b+R_1+R_2);$$

$$u_{RJ2}=R_b*(U_{J1}+U_{J2})/(R_a+R_b+R_1+R_2);$$

List of Quantities:

Quantity	Unit	Definition
R_r		Ratio measured between two resistors
U_{J1}	V	Josephson Voltage generated from JWS1
u_{RJ1}	V	Voltage across the 50-Ω resistors connected to the voltage lines of JWS1
U_{J2}	V	Josephson Voltage generated from JWS2
u_{RJ2}	V	Voltage across the 50-Ω resistors connected to the voltage lines of JWS2
U_F	V	Voltage read by the lock-in amplifier in the forward connection
U_R	V	Voltage read by the lock-in amplifier in the reverse connection
R_a	Ω	the 50-Ω resistors connected to the voltage lines of JWS1
R_b	Ω	the 50-Ω resistors connected to the voltage lines of JWS2
R_1	Ω	Resistance value of Resistor 1
R_2	Ω	Resistance value of Resistor 2

R_r: Result

	Uncertainty Budget for the Two-Terminal-Pair Josephson Impedance Bridge	PTB

U_{J1}: Type B normal distribution
Value: 1.514848645 V
Expanded Uncertainty: 0.000000001 V
Coverage Factor: 2

Voltage generated by JWS1 using a square wave at 70.235 GHz of 8192 Josephson junctions.

(70.235*8192/483597.9)*(4/pi)

u_{RJ1}: Temporary

Voltage across the 50-Ω resistors connected to the voltage lines of JWS1 due to the employment of the reflection compensation connection.

U_{J2}: Type B normal distribution
Value: 1.514902566 V
Expanded Uncertainty: 0.000000001 V
Coverage Factor: 2

Voltage generated by JWS1 using a square wave at 70.2375 GHz of 8192 Josephson junctions.

(70.2375*8192/483597.9)*(4/pi)

u_{RJ2}: Temporary

Voltage across the 50-Ω resistors connected to the voltage lines of JWS2 due to the employment of the reflection compensation connection.

U_F: Type B normal distribution
Value: 0.000005357 V
Expanded Uncertainty: 0.000000011 V
Coverage Factor: 1

U_R: Type B normal distribution
Value: -0.000001390 V
Expanded Uncertainty: 0.000000011 V
Coverage Factor: 1

R_a: Type B normal distribution
Value: 51.02 Ω
Expanded Uncertainty: 0.013 Ω
Coverage Factor: 1

Measurement uncertainty = ± 0.013 Ω

Contact resistance = ± 0.001 Ω

Temperature coefficients = 10 ppm/K

Date: 03/18/2010	File: 2T Uncertainty	Page 2 of 4

R_b: Type B normal distribution
Value: 51.36 Ω
Expanded Uncertainty: 0.012 Ω
Coverage Factor: 1

Measurement uncertainty = ± 0.012 Ω

Contact resistance = ± 0.001 Ω

Temperature coefficients = 10 ppm/K

R_1: Type B normal distribution
Value: 9999.937 Ω
Expanded Uncertainty: 0.004 Ω
Coverage Factor: 1

Temperature coefficients = 0.011 Ω/K

Temperature controlled enclosure at ± 1 mK

R_2: Type B normal distribution
Value: 9999.963 Ω
Expanded Uncertainty: 1 Ω
Coverage Factor: 1

Temperature coefficients = 0.011 Ω/K

Temperature controlled enclosure at ± 1 mK

Uncertainty Budget:

Quantity	Value	Standard Uncertainty	Degrees of Freedom	Sensitivity Coefficient	Uncertainty Contribution	Index
U_{J1}	1.514848645000 V	$500 \cdot 10^{-12}$ V	50	0.0	0.0	0.0 %
u_{RJ1}	$7.68957 \cdot 10^{-3}$ V	$1.99 \cdot 10^{-6}$ V				
U_{J2}	1.514902566000 V	$500 \cdot 10^{-12}$ V	50	0.0	0.0	0.0 %
u_{RJ2}	$7.74081 \cdot 10^{-3}$ V	$1.84 \cdot 10^{-6}$ V				
U_F	$5.3570 \cdot 10^{-6}$ V	$11.0 \cdot 10^{-9}$ V	50	-0.66	$-7.3 \cdot 10^{-9}$	50.0 %
U_R	$-1.3900 \cdot 10^{-6}$ V	$11.0 \cdot 10^{-9}$ V	50	-0.66	$-7.3 \cdot 10^{-9}$	50.0 %
R_a	51.0200 Ω	0.0130 Ω	50	not valid!	$-4.0 \cdot 10^{-12}$	0.0 %
R_b	51.3600 Ω	0.0120 Ω	50	not valid!	$560 \cdot 10^{-15}$	0.0 %
R_1	9999.93700 Ω	$4.00 \cdot 10^{-3}$ Ω	50	0.0	0.0	0.0 %
R_2	9999.96 Ω	1.00 Ω	50	$670 \cdot 10^{-15}$	$670 \cdot 10^{-15}$	0.0 %
R_r	$-2.632 \cdot 10^{-6}$	$10.3 \cdot 10^{-9}$	100			

	Uncertainty Budget for the Two-Terminal-Pair Josephson Impedance Bridge	PTB

Result: Quantity: R_r
Value: $-2.632 \cdot 10^{-6}$
Expanded Uncertainty: $\pm 21 \cdot 10^{-9}$
Coverage Factor: 2.0
Coverage: t-table 95%

Date: 03/18/2010	File: 2T Uncertainty	Page 4 of 4

Acknowledgements

First and foremost, I am heartily thankful to Prof. Dr. Meinhard Schilling who provided the opportunity for me to take on this project and made available his support in a number of ways. I owe my deepest gratitude to Dr. Chua Sze Wey who made this work possible by giving me the opportunity to pursue my PhD and gave constant encouragement and support even though he is ten thousand kilometers away. I am honored to work with one of the finest, Dr. Franz Joseph Ahlers, and appreciate greatly for his valuable guidance and brilliant advices. I'm always marveled by how he constantly manages to aspire like angels from heaven.

I offer my deepest gratitude to my supervisor, Dr. Ralf Behr, who has infused me throughout my thesis with his encouragement and knowledge and cookies. He helped me made the impossible possible, because he is like a wizard with awesome great magics. I am very grateful to Dr. Luis Palafox whom is always around to help me in many ways including making delicious paella for me.

I would like to thank PD Dr. Uwe Siegner for offering his time to read and assess my work. His compliments to me made me very happy and I am very delighted to know that he recognizes my work.

I am indebted to my many of my colleagues to support me like Dr. Jürgen Schurr, Dr. Hansjeorg Scherer, Veit Bürkel, Dr. Bryan Kibble, Dr. Franz Müller, Manfred Gardalla, Michael Busse, Gerhard Muchow, Dr. Alexander Katkov, Dr. Janni Nissilä, Johnathan Williams and Dr. Dale Henderson. They contributed greatly to the success of this thesis and they are always very friendly and helpful to me all the time.

I would like to thank A*STAR Singapore for funding and providing the opportunity for this thesis to be made possible, and the support from the international graduate school of metrology (IGSM) Braunschweig.

Lastly, to everyone who supported me in any respect during the completion of the thesis who were not stated by name here, I offer my sincerest gratitude and warmest blessings to you.

Curriculum vitae

Jinni Lee

Born on 20th March 1978, Singapore

1985 – 1990	Primary School Nan Chiau High School, Singapore
1991 – 1994	Secondary School Chung Cheng Secondary School, Singapore
1995	Monash University Foundation Year Taylors College, Melbourne, Australia
1996 – 1999	Bachelor of Computer Science and Engineering Monash University, Melbourne, Australia
2000 – 2001	Master of Telecommunications Melbourne University, Melbourne, Australia
2001 – Present	Employed by A*STAR Singapore as a metrologist in the Electromagnetic Department Singapore
May 2007 – May 2010	Pursuing PhD with PTB on "Programmable Josephson Arrays for Impedance Measurements" Braunschweig, Germany

Declaration

This thesis is a presentation of my original research work. Wherever contributions of others are involved, every effort is made to indicate this clearly, with due reference to the literature, and acknowledgement of collaborative research and discussions.

I confirm that:

1. This work was done wholly or mainly while in candidature for a research degree at this University;

2. Where any part of this thesis has previously been submitted for a degree or any other qualification at this University or any other institution, this has been clearly stated;

3. Where I have consulted the published work of others, this is always clearly attributed;

4. Where I have quoted from the work of others, the source is always given. With the exception of such quotations, this thesis is entirely my own work;

5. I have acknowledged all main sources of help.